Data assimilation of forest status using Sentinel-2 data and a process-based model

Minunno, Francesco

Elsevier B.V.
2025-03-15

Minunno, F, Miettinen, J, Tian, X, Häme, T, Holder, J, Koivu, K & Mäkelä, A 2025, 'Data assimilation of forest status using Sentinel-2 data and a process-based model', Agricultural and Forest Meteorology, vol. 363, 110436. https://doi.org/10.1016/j.agrformet.2025.110436

http://hdl.handle.net/10138/592801
10.1016/j.agrformet.2025.110436

Agricultural and Forest Meteorology 363 (2025) 110436

Contents lists available at ScienceDirect

Agricultural and Forest Meteorology

journal homepage: www.elsevier.com/locate/agrformet

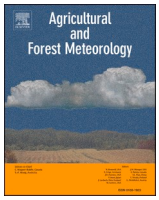

Data assimilation of forest status using Sentinel-2 data and a process-based model

Francesco Minunno [a,*], Jukka Miettinen [b], Xianglin Tian [c], Tuomas Häme [b], Jonathan Holder [a], Kristiina Koivu [a], Annikki Mäkelä [a]

[a] Department of Forest Sciences, University of Helsinki, Helsingin Yliopisto, Finland
[b] VTT Technical Research Centre of Finland, Espoo, Finland
[c] College of Forestry, Northwest A&F University, Yangling, China

ARTICLE INFO

Keywords:
Forest carbon monitoring
Data assimilation
Process-based modelling
Bayesian
Analysis
forest C balance

ABSTRACT

Spatially explicit information of forest status is important for obtaining more accurate predictions of C balance. Spatially explicit predictions of forest characteristics at high resolution can be obtained by Earth Observations (EO), but the accuracy of satellite-based predictions may vary significantly. Modern computational techniques, such as data assimilation (DA), allow us to improve the accuracy of predictions considering measurement uncertainties. The main objective of this work was to develop two DA frameworks that combine repeated satellite measurements (Sentinel-2) and process-based forest model predictions. For the study three tiles of 100 × 100 km^2 were considered, in boreal forests. One framework was used to predict forest structural variables and tree species, while the other was used to quantify the site fertility class. The reliability of the frameworks was tested using field measurements. By means of DA we combined model and satellite-based predictions improving the reliability and robustness of forest monitoring. The DA frameworks reduced the uncertainty associated with forest structural variables and mitigated the effects of biased Earth Observation predictions when errors occurred. For one tile, Sentinel-2 prediction for 2019 (s2019) of stem diameter (D) and height (H) was biased, but the errors were reduced by the DA estimation (DA2019). The root mean squared errors were reduced from 5.8 cm (s2019) to 4.5 cm (DA2019) and from 5.1 m (s2019) to 3.3 m (DA2019) for D (sd = 4.33 cm) and H (sd = 3.43 m), respectively. For the site fertility class estimation DA was less effective, because forest growth rate is low in boreal environments; long term analysis might be more informative. We showed here the potential of the DA framework implemented using medium resolution remote sensing data and a process-based forest model. Further testing of the frameworks using more RS-data acquisitions is desirable and the DA process would benefit if the error of satellite-based predictions were reduced.

1. Introduction

The increased prominence of forests in climate- change mitigation and bioeconomy strategies and the increasing importance of sustainability in forest policies brings new challenges to forest management. Forests have a prominent role in the success of major initiatives, such as the European Green Deal (European Commission 2019), the Paris Agreement, and the Sustainable Development Goals of the United Nations. At the same time, forests are facing environmental challenges due to changing climatic conditions (e.g. storms, drought, pest attacks) (Nabuurs et al., 2013; Reyer et al. 2017) and increasing demand for both wood and non-wood forest products (Verkerk et al. 2022). Furthermore, forestry stakeholders have numerous legal and voluntary obligations (e.g. certification schemes) to monitor and report the usage and status of forests. In this situation, acquiring up-to-date spatially explicit information on forest characteristics is more important than ever.

Up-to-date information on the current status of forests is not only needed for monitoring and operational planning purposes but also forms a basis for future management planning and policy formulation, supporting decision making from small-scale forest management to large-scale forest policies. Forecasting and planning use models that in practical forestry are largely empirical models based on statistical fitting of measurements of forest characteristics (Hynynen et al. 2002; Kallio et al. 2016; Eriksson and Bergh 2022; Lämås et al., 2023). Process-based

* Corresponding author.
E-mail address: francesco.minunno@helsinki.fi (F. Minunno).

https://doi.org/10.1016/j.agrformet.2025.110436
Received 14 May 2024; Received in revised form 29 January 2025; Accepted 2 February 2025
Available online 8 February 2025

models (PBM) derive forest growth from ecological processes, which broadens the scope of future projections by including the impacts of different environmental conditions on forest processes (Fontes et al. 2010; Lukash et al. 2018; Minunno et al. 2019). However, to be usable for spatially explicit future projections in large areas, models require accurate and spatially detailed information on forest characteristics as input data.

Most countries have a National Forest Inventory (NFI) and other wide-scale field measurement (e.g., permanent growth experiments, fertilization trials) campaigns that provide information on forest status to support management planning and policy decisions. However, field-plot measurements alone do not provide spatially explicit predictions of forest characteristics in < 30 m spatial resolution. The content and quality of NFI measurements also vary widely between countries (McRoberts et al. 2009). Remotely sensed datasets are increasingly used in large forest inventories (Kangas et al. 2018), due to the increased availability of remotely sensed data at finer resolution. Earth Observation (EO) based approaches that combine field data with satellite observations can be used to predict forest characteristics in a spatially explicit manner for large areas (e.g. Breidenbach et al. 2020). However, the accuracy of EO-based forest variable predictions at appropriate spatial resolution (10–30 m) has thus far been relatively modest, with RMSE between 40 and 60 % of the mean for several structural forest variables such as basal area, mean diameter at breast height, mean height, stem volume (Astola et al. 2019; Häme et al. 2013; Antropov et al. 2017; Sánchez-Ruiz et al. 2019, Santoro et al., 2019b, Ahmadi et al. 2021).

There is an increasing body of studies in Earth sciences showing that measurement accuracy can be improved and uncertainties can be quantified and reduced by data assimilation (DA) (Montzka et al. 2012, Calvet et al., 2019, Mohamedou et al. 2022). DA combines observations and models while also considering the associated error. Using DA, model parameters are updated to make the predictions agree with field observational data (Khaki et al. 2020) and vice versa. The history of the observations is accounted for through the model to reduce the impacts on estimation of possible noise in the observations (Junttila et al. 2008; Leroux et al. 2018). Although many computational methods have been developed and applied (Montzka et al. 2012), the Kalman filter is the most common method used for DA. DA has already been extensively and successfully applied in many fields of earth sciences, such as meteorology (Rabier, 2005) and hydrology (Khaki et al. 2020),

In the last few years, DA based on earth observation data has also been increasingly adopted into forest variable estimation from large areas (Hou et al. 2019; Breidenbach et al. 2020, Lindgren et al., 2022a, 2022b). While most of these studies focus on monitoring the current state of the forest, fewer applications have utilised sequential EO data in combination with predictive simulation models (Mohamedou et al. 2022). Such approaches can be hampered by the high computational load of combining DA with forward simulations of forest variables (Mohamedou et al. 2022), as concluded on the basis of previous studies applying empirical forest growth models (Nyström et al. 2015; Lindgren et al. 2017). However, DA is challenging when more computationally expensive models, such us process-based forest models are applied to large areas (>100 km^2) at < 30 m spatial resolution (Dietze et al., 2013).

Using DA in sequential forest variable prediction requires that the applied simulation model accounts for the change of state over the observation interval. Forest simulation models usually describe the forest state in terms of structural variables, such as species proportions or plant functional type, mean height, tree diameter, basal area, leaf area index (LAI) and tree age. The change of state depends on prevailing climatic and edaphic factors, together embedded in the concept of site productivity (Skovsgaard and Vanclay 2008). While climate variables are generally available through measurement networks or climate models, estimating the edaphic factors is considered a key limiting issue in the applications of remotely sensed data for forest growth prediction (Knyazikhin et al. 2013; Waring et al. 2016). Foresters quantify site fertility with the so-called site index (i.e. the dominant canopy height reached by a reference age) (Skovsgaard and Vanclay 2008). Although site index is difficult to estimate directly if tree age is not known, age-independent methods of estimating site quality have also been developed (Skovsgaard and Vanclay 2008). One of these is the ground vegetation-based site classification system used in Finland (Cajander 1949), which has also been linked with site index (Vuokila and Väliaho, 1980). This has already allowed for advances in estimating site fertility class from EO data (Häme 1984; Häme et al. 2023).

Based on its definition, DA is helpful if there are repeated remotely sensed measurements available for a forest area. It is then possible to initialize the model with the first data acquisition and forecast the state of the forest to the date of the next data acquisition. The two sources of information are combined considering their relative uncertainty. The new prediction constitutes the starting point for a new DA, and the process can be repeated every time new data become available. EO datasets suitable for this kind of repeated forest observations are available free of charge at a resolution of 10–30 m. These include optical datasets (such as Sentinel-2 and Landsat 8) and radar datasets (such as the C-band Sentinel 1). Several authors have used 10–30 m EO based estimates to create spatially explicit maps of forest structural variables (such as tree species, height, and stem volume) (Astola et al. 2019; Häme et al. 2013; Antropov et al. 2017, Miettinen et al., 2021) and site fertility indices (Häme 1984; Tomppo 1992; Moran et al. 2000; Rahimzadeh-Bajgiran et al. 2020; Häme et al. 2023,) that can be used as input for process-based ecosystem modelling. In particular, the European Space Agency Sentinel-2 satellite, with its 10 wavelength bands in 10–20 m spatial resolution and high temporal frequency (5-day revisit period at the equator, 2–3 days in mid latitudes), provides useful data for large-scale forest monitoring.

The main objective of this study is to build and test two frameworks for data assimilation of satellite measurements at 10 meter resolution in combination with a simple process-based model, PREBAS (Minunno et al. 2019). We implemented:

1) a framework for the prediction of site fertility that is site specific and remains relatively stable over time;
2) a framework for the prediction of forest structural variables that dynamically change over time.

2. Materials and methods

2.1. Satellite data

Sentinel-2 Level 2A (L2A) satellite data (together with field measurements) were used to estimate forest variables that are key state variables in the process-based ecosystem model used in this study. With two satellites on sun-synchronous orbits and a 290 km swath width, the Sentinel-2 Multi-Spectral Instrument (MSI) sensor provides 2–3 days imaging frequency in Europe. The sensor has 13 spectral bands with 10 m (four bands), 20 m (six bands) and 60 m (three bands) spatial resolutions. The Level 2A product provides atmospherically corrected surface reflectance, distributed in tiles of 110 × 110 km^2. Three Sentinel-2 tiling grid tiles 'Vaasa' (grid code 34VEQ), 'Tampere' (35VLJ), and 'Oulu' (35WMN) were used in the study, providing a north-south spread through the boreal zone (Fig. 1). The sites were selected considering the availability of field data and the availability of early (2016) Sentinel-2 data.

For each of the three tiles, Sentinel-2 L2A composite images were created for 2016 and 2019 using imagery acquired between 1st of June and 15th of September. The number of images varied from <10 to 20 for each of the three tiles. The observations covered the entire compositing period, which was limited to the growing season to reduce the effects of seasonal variation in the composite imagery. Each ground resolution element of the image was evaluated according to the following four criteria: cloudiness, haze, cloud shadows, and resemblance to usual

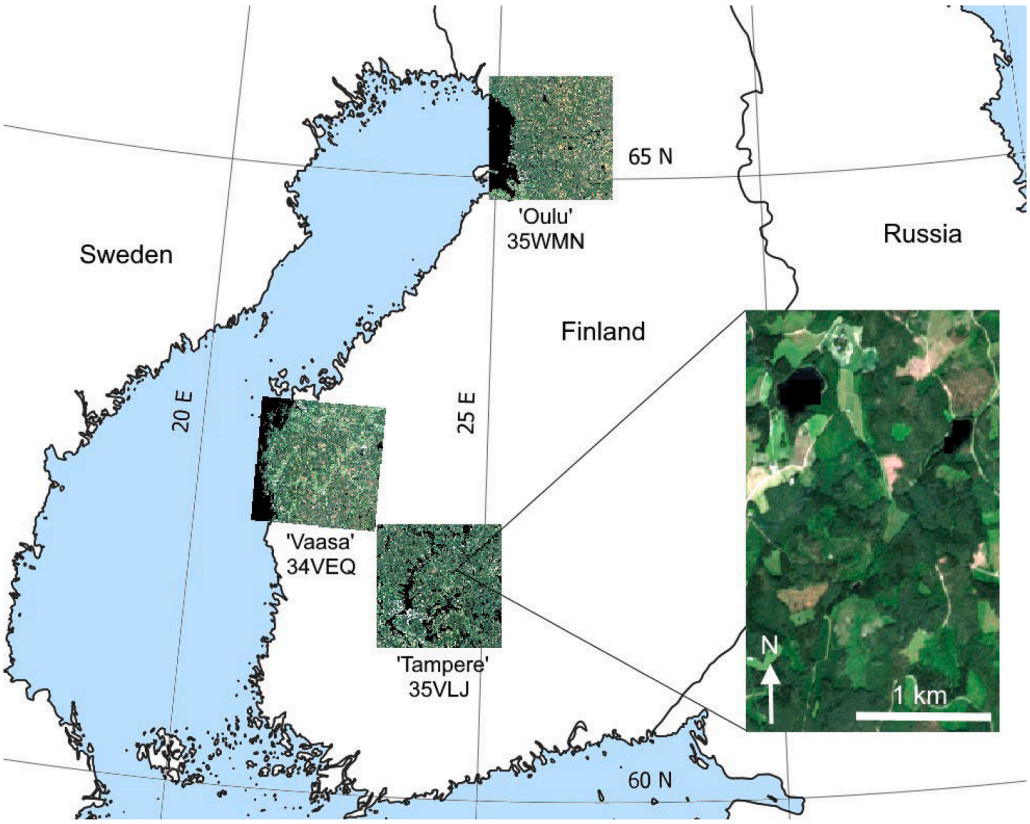

Fig. 1. Location of study sites with Sentinel-2 L2A composite images. The inset shows a detail of the 'Tampere' (tiling grid 35VLJ) image.

observation in the location (based on a reference mosaic built from visually selected cloud free imagery). Based on the evaluation, a weight was given for each observation and these weights were used to average the observations to produce the final image. The compositing approach is described in detail in Miettinen et al. (2021). The final composite images included seven spectral bands (B02 Blue 0.49 μm, B03 Green 0.56 μm, B04 Red 0.67 μm, B05 Red Edge 1 0.71 μm, B08 NIR 0.84 μm, B11 SWIR 1.61 μm and SWIR 2.19 μm). These bands were selected to be used based on earlier results on optimal set of bands for boreal forest variable prediction (Astola et al. 2019). All bands were resampled to 10 m spatial resolution using the nearest neighbour resampling.

2.2. Field data

Field plot measurements were used as training data for the forest variable model creation and reference data for accuracy assessment. Altogether, 5054 field plots were used, 2508 for the creation and evaluation of the 2016 model, and 2546 for the 2019 model. The field data plots were measured in 2016 and 2019 by the Finnish Forest Centre (https://www.metsakeskus.fi/node/321). The following three different plot radii were used in the measurements: 9 m in young and mature managed forests with a relatively high tree density; 12.62 m in forests with a low stem density but usually high volume due to the mature development stage; and 5.64 m in seedling stands. Before use of the field plot data, all plots were visually screened on the Sentinel-2 composite images, and all plots that were located in areas with clear atmospheric disturbance were removed. Every third plot was randomly selected for accuracy assessment, while the remaining two-thirds were used for model training. To take into account the varying sizes of the field plots, intersections with raster data were conducted with shapefiles representing the plots as circular polygons reflecting the plot size. Weighted averages of the raster values were calculated based on the proportion of coverage of each pixel within the plot polygon. This approach was applied to both the spectral value extraction during the forest variable prediction as well as the map value extraction for accuracy assessment.

Eight variables were extracted from the field plot database and used in the forest structural variable model creation. These were Basal area (G), mean Diameter at breast height (D), Height (H), Volume (V), Scots pine (*Pinus sylvestris* L.) proportion of growing stock volume (R_P, Norway spruce (*Picea abies* Karst.) proportion (R_S), Broadleaf tree proportion (R_B), and fertility class (Site). The height was calculated as basal area weighted average height. The standard Finnish site-type classification estimating site fertility based on ground vegetation was used (Cajander, 1949). The classification includes eight classes in total arranged according to decreasing fertility. >99 % of forest land in Finland is assigned to the first five classes, which were used in the analysis (Korhonen et al. 2017) (Table 2). While the generic names of the classes refer to upland site types, we classified forested and drained peatlands in corresponding site classes based on their productivity. All of the analyses conducted in the study were limited to forest area, as outlined by the Forest Mask (Metsämaski) of the Finnish Forest Centre (https://www.metsakeskus.fi/en/about-us/the-finnish-forest-centre).

2.3. Probability forest structural variable prediction

The *Probability* forest classification and prediction approach (Häme et al. 2001) was used to derive the forest structural variable predictions that were used for initialising the simulations with the process-based ecosystem model. The creation of the maps has been described in detail in Miettinen et al. (2021) and only the key features of the process are repeated here. The workflow included three main phases (clustering, model creation, and prediction; Fig. 2). The process started with a clustering of the input images with maximum likelihood clustering into 60 clusters. A model was then created by associating the field measurements with the clusters. The forest variable values for each cluster were computed as median (for G, D, H and V) or mean (for R_P, R_S, R_B and

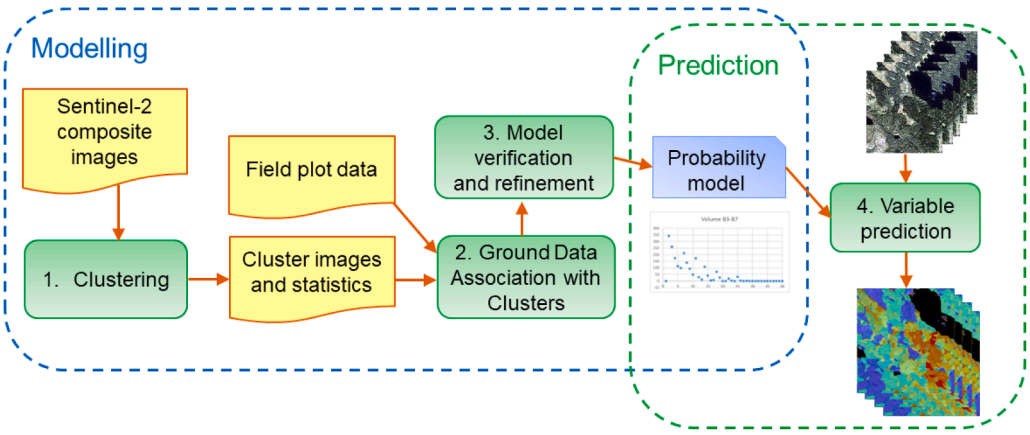

Fig. 2. Workflow of the forest structural variable prediction method (modified from Miettinen et al., 2021).

fertility) of all field measurements belonging to this cluster, and the spectral statistics (of the surface reflectance) of the clusters were recorded. The model was subsequently evaluated and refined. In the final phase, predictions for each ground resolution element were calculated as the weighted average of the five clusters to which the Euclidean distance from the given element was closest in the multi-spectral space. The weights were the probabilities of the ground resolution element belonging to the cluster (Häme et al. 2001; Eq. (1)).

$$f(x) = \sum_{c=1}^{N} P(c \vee x) f_c, \quad (1)$$

where $f(x)$is the estimated target variable value for spectral vector x, $P(c \vee x)$ is the probability for spectral vector x to belong to cluster c, f_c is the reference target variable value for cluster c, and N is the number of clusters used in the prediction (five in this study).

Note that the fertility class was also treated as a continuous variable at this point, since it was calculated as percentages of fertility classes in each cluster (based on the number of plots fallen into the cluster). The fertility class was subsequently converted into a category variable by choosing the fertility class with the highest percentage as the fertility class for a given spatial unit.

2.4. PREBAS and model emulator

The forest model used in this study is PREBAS (Minunno et al., 2019), which is a combination of a light use efficiency model, PRELES (Mäkelä et al., 2007; Peltoniemi et al., 2015), and a forest growth model (CROBAS, Mäkelä, 1997; Valentine and Mäkelä, 2005) based on the carbon budget and pipe model theory. PREBAS predicts carbon and water balances and the growth of forests and has been calibrated for the European boreal region (Minunno et al., 2016, 2019). Model inputs are climatic variables at daily time step (temperature mean, solar radiation, precipitation, vapor pressure deficit, CO_2 concentration), forest initial state (basal area, average height, diameter at breast height), and site parameters (fertility class, soil depth, wilting point, field capacity). PREBAS can model simple monospecific and even aged plantations as well as more complex forest structures, such as mixed and uneven-aged forests. PREBAS showed robust performances in even aged plantations (Minunno et al., 2019), while for mixed uneven-aged stands the model has not been extensively tested.

In this study, we used weather inputs provided by the forest meteorological institute at 10 km grid resolution. PREBAS was initialized using the structural forest variables predicted with the Probability method using Sentinel-2 and field data. The forest structure inputs included basal area (G), diameter at breast height (D), height (H), pine proportion (R_P), spruce proportion (R_S), broadleaved species proportion (R_B), and fertility class.

We created model emulators (modEm) that mimicked PREBAS outputs for the different tiles to reduce the computational load. The emulators were regression models fitted to simulate PREBAS outputs (G,D,H, R_P,R_S,R_B) at the time of the second satellite measurement (2019, t_2). The structural forest variables and fertility class at the first satellite measurement (2016, t_1) were used as independent variables. PREBAS was initialized with the satellite based predictions of forest structural variables in 2016. The emulators were fitted using PREBAS predictions for 2019.

$$Y_i = f(X_1, \ldots, X_k) + \epsilon_i \quad (2)$$

The dependent variables (Y_i) were G, D, H, R_P, R_S, R_B and volume increment (dV) at t_2. The independent variables were H, D, stand density index (SDI $N\left(\frac{D}{25}\right)^b; b = -1.605$), $G \times H$, species shares of basal area G (G_P, G_S, G_B for pine, spruce and broadleaved, respectively) at t_1, and fertility class. The regressions were fitted minimizing the root mean squared errors.

2.5. Data assimilation frameworks

We implemented two DA frameworks that, through the implementation of a few steps, allowed combination of structural variable predictions from Sentinel-2 data and forest model predictions. One framework was used to update the forest structural variables (state variables: G, D, H, G_P, G_S, G_B) (ForVarDA, Fig. 3); the other framework was used to update the estimates of site fertility class (STDA, Fig. 4).

Data assimilation updates a system's state by integrating predictions with new observations. It commonly uses a Bayesian approach, which combines prior information and new data to update probabilities through Bayes' theorem. The Kalman filter (KF) analytically adjusts the state's mean and covariance, but struggles with high-dimensional systems. The Ensemble Kalman Filter (EnKF) simplifies this by using a Monte Carlo method, generating multiple predictions from the initial state to better handle uncertainty. A comprehensive description of the Ensemble Kalman Filter (EnKF) and its application in this study can be found in Appendix A5.

Example codes of the two frameworks implemented in this study are available on github (https://github.com/ForModLabUHel/DaexampleCode).

We excluded areas likely to have undergone forest management between the acquisition dates of the composite tiles, as management was not included in our growth modeling framework. The procedure followed to identify the managed areas are described in Appendix A6.

2.5.1. Data assimilation workflow for forest structural variables

The DA workflow for the forest structural variables consists of 5 steps

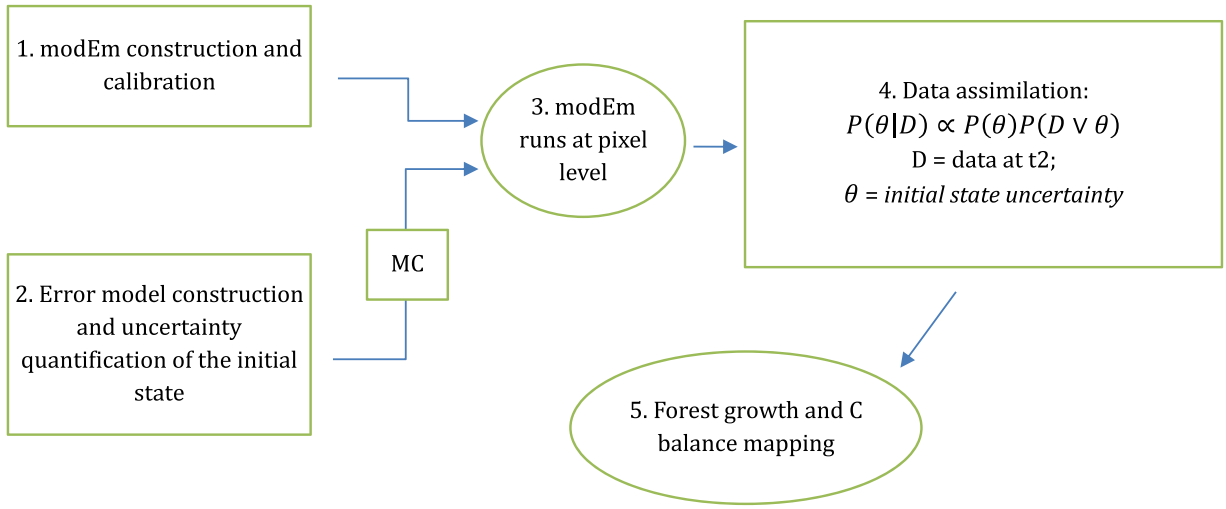

Fig. 3. Flowchart for the data assimilation of forest structural variables. *P(θ|D)*: posterior probability distribution of forest structural variables integrating EO based predictions from 2016 to 2019 and model predictions; *P(θ)*: prior distribution, given by the initial state uncertainty of Sentinel-2 2016 predictions propagated to 2019 by means of PREBAS predictions; *P(D|θ)*: likelihood function calculated using forest structural variables obtained from model predictions and Sentinel-2 predictions for 2019.

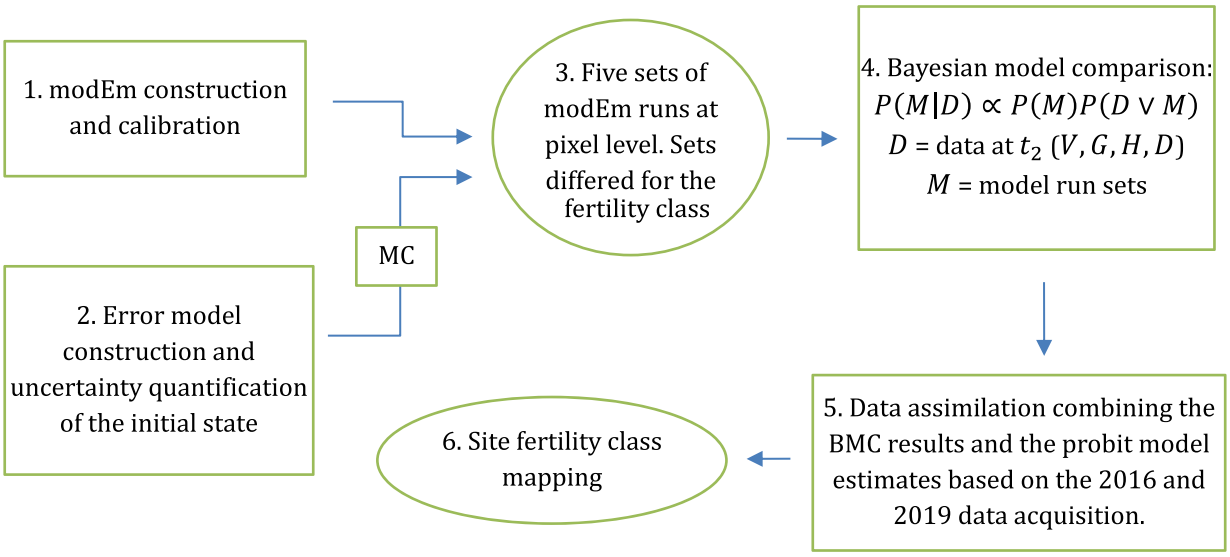

Fig. 4. Flowchart for the data assimilation framework of site fertility class. *P*(M|*D*): probability of site fertility class being correct, based on model runs; *P*(M): prior probability of site fertility class (all fertility classes had the same prior probability); *P*(*D*|M): integrated likelihood calculated using forest structural variables calculated by model predictions and Sentinel-2 predictions for 2019.

(Fig. 3); steps 2 to 5 were implemented at spatial resolution level (10 × 10m):

1. Emulator calibration;
2. Uncertainty quantification;
3. Forecast step;
4. Data assimilation;
5. Map production.

2.5.1.1. Emulator calibration. In step 1, the emulators (Eq. (1)) were fitted using PREBAS predictions for time 2; emulator calibrations were performed for each tile. We randomly extracted 20 000 ground resolution elements; PREBAS was initialized with Sentinel-2 based predictions for 2016 (s2016) and its predictions (*G*,*D*,*H*, species coverage) for 2019 were used to fit the emulators (Eq. (1)). The site fertility class was sampled from the posterior distribution obtained by the data assimilation framework, as described below (section 2.5.4).

2.5.1.2. Uncertainty quantification. In step 2, we propagated the error of the forest structural variables predictions for 2016 at the ground resolution element level. Using the residuals between the observed (2016 field campaign measurements) and the satellite-estimated values (s2016) of forest structural variables, we fitted a multivariate normal distribution (errDistr). For each spatial unit, we drew 1000 samples from errDistr and added to the s2016 predictions. To avoid negative values, we used a non-negative probability distribution sampling strategy presented in Appendix A1.

2.5.1.3. Forecast step. In step 3, we ran the emulator 1000 times for each 10 m x10 m pixel, using the inputs generated in step 2. By means of the emulator runs, we computed the forest structural variables at 2019 with the associated uncertainty.

2.5.1.4. Data assimilation. In step 4, we combined the emulator forecasts with satellite-based predictions at 2019 using the Bayesian approach. The forecasts generated in step 3 were used to construct the prior distribution as a multivariate normal distribution of the forest structural variables. The new estimates at 2019 were encoded in the likelihood function using the same approach as in step 2, i.e. we constructed an error distribution on the basis of the residuals between the field measurements and the Sentinel-2 predictions of 2019 and fitted a multivariate normal distribution. The posterior was calculated using the Kalman filter as an analytical solution to compute the moments of forest structural variables.

2.5.1.5. Map production. In step 5, we generated maps of carbon balance and forest growth and their relative uncertainties using the maximum a posteriori (MAP) estimates and their relative uncertainty expressed by standard deviation.

2.5.2. Data assimilation workflow for site fertility

The data assimilation workflow for site fertility class estimates consists of six steps (Fig. 4); steps 2 to 6 were implemented at 10 m resolution:

1. Emulator calibration;
2. Uncertainty quantification;
3. Forecast step;
4. Bayesian model comparison;
5. Data assimilation;
6. Map production.

2.5.2.1. Emulator calibration and uncertainty quantification. The first two steps were the same as in the forest structural variable assimilation framework.

2.5.2.2. Forecast step. In step 3, for each ground resolution element, we conducted 5 sets of emulator runs. Similarly to step 3 of the previous framework, we ran the emulators 1000 times at 10 m x 10 m resolution, considering the uncertainty of the inputs. Here, we ran the sample 5 times using different site fertilities, i.e. the fertility class varied from 1 to 5 for each set.

2.5.2.3. Bayesian model comparison. In step 4, we calculated the integrated likelihood for each set of runs using the forest structural variables at t_2 ($G, H, D,$ and V). By means of Bayesian model comparison (BMC), we compared the performance of the different run sets and calculated the probability for each set of being the correct one (vanOijen et al., 2013; Minunno et al., 2013). In this way, on the basis of model predictions, we quantified the probability of each fertility class of being the correct one. A more detailed description of BMC and its application in this study is provided in appendix A2.

2.5.2.4. Data assimilation. For each spatial unit we had three discrete probability distributions for the 5 fertility classes; one based on the results of the Bayesian model comparison and the other two were based on the satellite predictions from 2016 to 2019. In step 5, we updated the site fertility class distributions using the three sources of information.

2.5.2.5. Map production. In step 6, we generated maps of fertility class and their relative uncertainty based on the results of data assimilation.

2.6. Validation of the forest structural variables

Accuracies of the forest structural variable models were evaluated using the following accuracy metrics:

For continuous forest variables (i.e. all but fertility class), Root Mean Square Error (RMSE) and bias of the estimates (Eq. (3), Eq. (4)):

$$\mathrm{RMSE} = \sqrt{\Sigma_i} \tag{3}$$

$$\mathrm{BIAS} = \frac{\Sigma_i (y_i - \hat{y}_i)}{n} \tag{4}$$

where y represents the field measurements, $\hat{y}$ represents the estimated values, and n is the number of samples. Relative metrics, i.e. RMSE% and BIAS%, were computed using the mean value of the variable across the sites.

2.6.1. Analysis of the error components

For the error analysis, we used the mean squared error (MSE) decomposition proposed by Kobayashi and Salam (2000). MSE is given by the following three components: squared bias (s_b), squared difference between standard deviations (s_d), and lack of correlation weighted by the standard deviations (l_c):

$$MSE = \overline{(M - O)^2} = s_b + s_d + l_c \tag{5}$$

$$s_b = (\overline{M} - \overline{O})^2 \tag{6}$$

$$s_d = (\sigma_M - \sigma_O)^2 \tag{7}$$

$$l_c = 2(\sigma_M \sigma_O)(1 - r) \tag{8}$$

where M refers to predictions (from S2, PREBAS, DA), O to the observations (field measurements), σ is the standard deviation, and r is the correlation between the simulated and the observed data. The bias error indicates the average mismatch between model and data; the variance error quantifies the ability of the model to cover the variability of the data. l_c measures the ability of the model to reproduce the pattern of the fluctuations in the data, i.e. the correlation between model and data.

3. Results

3.1. Data assimilation framework for forest structural variables

Basal area, average diameter at breast height, average height, and species distribution predictions were updated for each ground resolution element of the areas considered in this study. Data assimilation results were calculated by means of the EnKF, combining PREBAS model forecasts to 2019 (m2019) and the satellite-based predictions for 2019 (s2019) (Fig. 5). Even when m2019 and s2019 predictions were inconsistent, DA2019 results had a reduced uncertainty (Fig. 5, first row).

Forest variable predictions achieved through Sentinel-2 data, model forecasts, and data assimilation showed consistent patterns across the tiles; the distribution of the variable showed similar major peaks, even though s2016 estimates were shifted towards lower values (Fig. 6a and 6b). Modelled growth rates looked realistic; the magnitude of the forecast variables (G, D, and H) and satellite-based predictions for 2019 were consistent, with the northernmost tile (Oulu) showing lower growth rates compared to the other two tiles (Fig. 6a).

Deciduous trees were the least abundant species in all tiles; pine had the highest percentage cover in Vaasa and Oulu (Fig. 6b). The patterns of species coverage over the tiles were consistent between the different data sources (m2019, s2019, DA2019) (Fig. 6b).

Data assimilation significantly reduced the uncertainty of all forest structural variables (Fig. 7a) and species coverage (Fig. 7b). For the uncertainty propagation from the first satellite measurement (s2016) to the model predictions of 2019 (m2019), the modelled uncertainty of basal area was higher than the s2016 uncertainty in the two most productive tiles (Vaasa and Tampere) (Fig. 7a). In contrast, m2019 uncertainty was lower than s2016 uncertainty of average height and diameter at breast height (Fig. 7a). The modelled species coverage uncertainty (m2019) was always lower than the s2016 uncertainty (Fig. 7b). Species

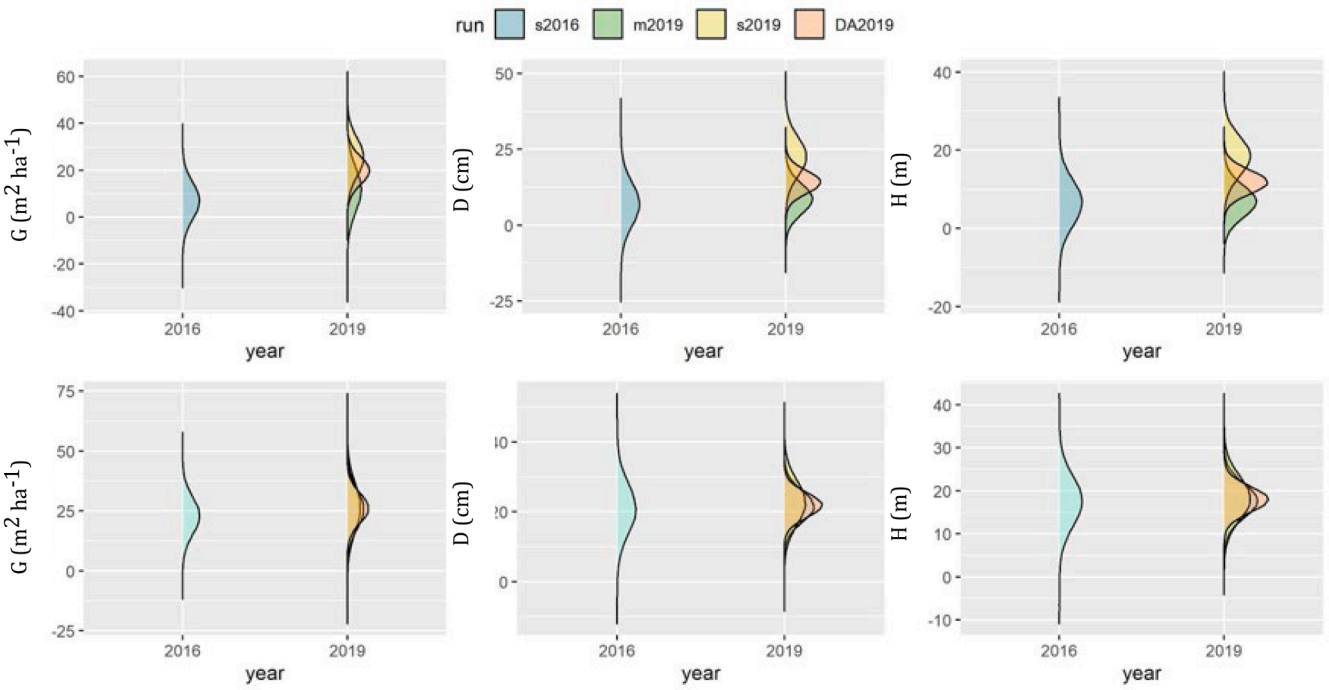

Fig. 5. Example of data assimilation at 10 m resolution. The blue, green, and yellow distributions represent the uncertainty of Sentinel-2 satellite-based predictions for 2016 (s2016), model predictions for 2019 (m2019), and Sentinel-2 predictions for 2019 (s2019), respectively. The distribution of the data assimilation results is reported in red (DA2019). The first row of the figure panels is an example of data assimilation for a ground resolution element where m2019 and s2019 diverged; the second row shows results from a ground resolution element where m2019 and s2019 predictions were consistent.

coverage uncertainty of s2019 was always in between s2016 and m2019 uncertainty (Fig. 7b).

3.2. Data assimilation framework for site fertility

Three sources of information were used for the prediction of the site fertility class at 10 by 10 meter resolution. By means of data assimilation, we integrated all the sources using a probabilistic approach. On a pixel basis, we calculated the probability of each site class being correct.

The DA and the two satellite-based predictions of site class showed consistent results (Fig. 8). The site fertility class with the highest probability was the same for DA2019, s2016, and s2019 in most of the ground resolution elements. Only in some cases was there a difference of one class between the highest probability class of different estimates (data not shown).

The site fertility classes 3 and 4 were the most common satellite predictions over the tiles (Fig. 8); the results of Bayesian model comparison were not informative and all site classes achieved similar probability (Fig. 8). The results of data assimilation showed distributions similar to the satellite estimate distributions, but with lower kurtosis (Fig. 8).

3.3. Validation

Forest structural variables and the fertility classes for 2019 were estimated using three sources. These were model forecasts based on forest state derived from Sentinel-2 data acquired in 2016 (m2019), Sentinel-2 based predictions from 2019 data acquisition (s2019), and data assimilation (DA2019). The accuracy of each estimate was evaluated using an independent field dataset collected during the Finnish Forest Centre 2019 field measurement campaign (Table 1) (see also appendix A4).

The model-based predictions (m2019) had higher error than the Sentinel-2 based (s2019) or assimilated (DA2019) estimates for the Tampere and Vaasa tiles. In the Oulu tile, the Sentinel-2 based predictions (s2019) of D and H had significantly higher error than m2019 and DA2019 (Tables 3a and 3b).

For the predictions of D and H of the two southernmost tiles (Tampere and Vaasa), the RMSE of the data assimilation was lower than the error of m2019 and s2019 (Fig. 9, Table 3a and b). For the Oulu tile, the basal area RMSE of DA2019 was the highest, even though the differences with m2019 and s2019 errors were small (0.1 and 0.3 m^2 ha^{-1}, respectively). In all other cases, the DA2019 RMSE was similar or equal to the smallest error (Fig. 9, Table 3a and b).

For the Tampere and Vaasa tiles, the lack of correlation (l_c) was the error component with the highest weight for all variables. Data variability (s_d) had a lower weight, while the bias component (s_b) was negligible (Fig. 9).

The bias component assumed significant values for the Oulu tile, in particular for the s2019-based predictions of *D* and *H* (Fig. 8). The bias error propagated throughout the Oulu tile (Fig. 10). However, the data assimilation results of *D* and *H* for the Oulu tile were closer to the m2019 forecasts than the s2019 predictions (Fig. 10).

Species proportions estimations were the variables characterized by the highest error (Tables 4a and 4b).

The fertility classes were estimated with a total accuracy rate that varied between 55 % (S2–2016) and 63 % (S2–2019) (Table 5) and the error of the fertility class predictions was of 1 class in most of the cases (Fig. 2. A4 in appendix A4).

4. Discussion

In this study, we implemented two data assimilation frameworks that allowed for spatially explicit estimates of site fertility classes and forest structural variables with their associated uncertainty, combining multiple sources of information rather than using only the most recent data collection. The new maps included all the available information acquired by repeated Earth observations (2016 and 2019) and model simulations.

To our knowledge, this is the first time that a data assimilation

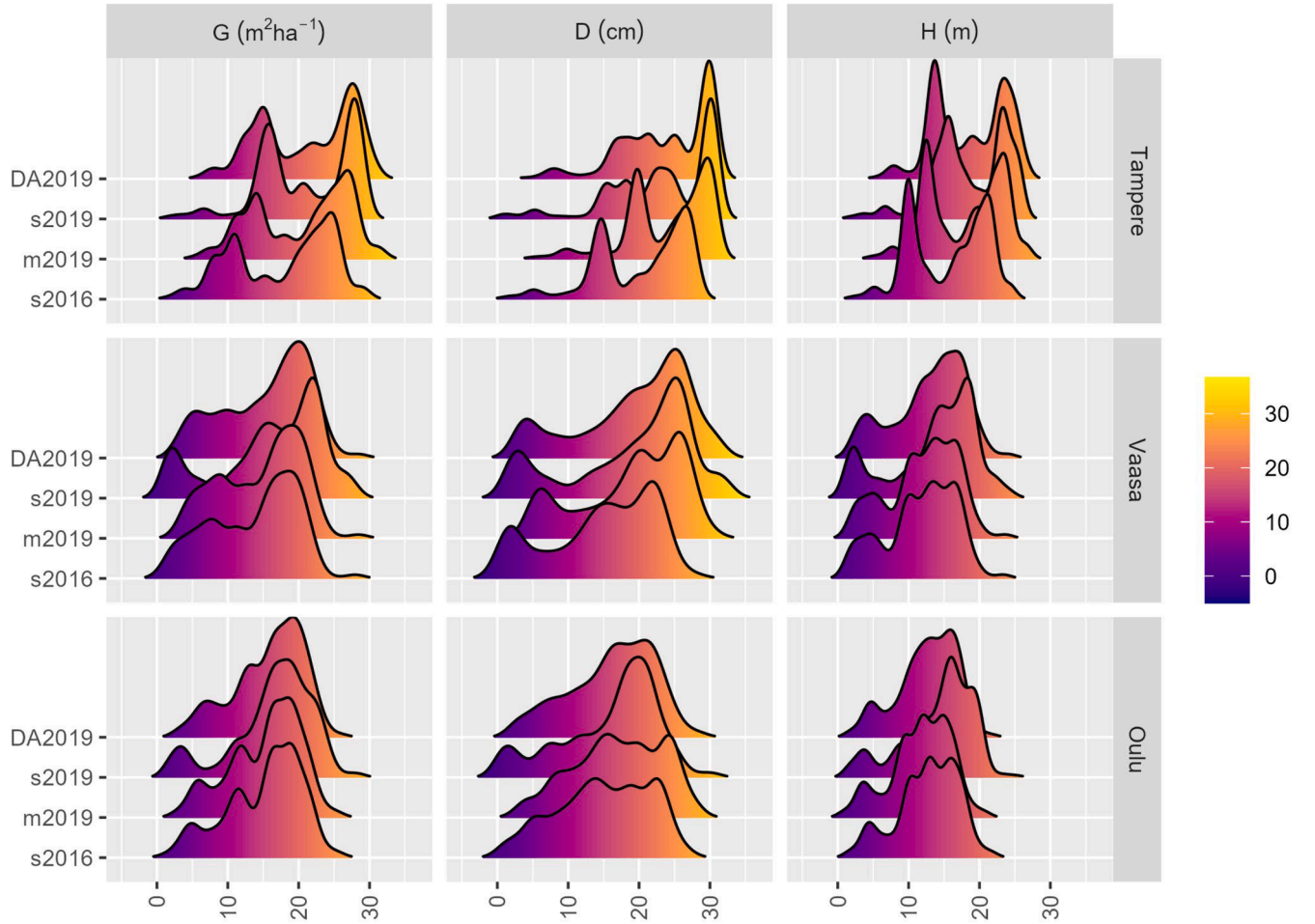

Fig. 6a. Distribution of the highest probability predictions for each ground resolution element of average height (*H*), average diameter at breast height (*D*), and basal area (*G*) over the three tiles. The distributions were drawn from satellite-based predictions (s2016, s2019), model-based predictions (m2019), and data assimilation (DA2019). The color scale corresponds to the value of the x-axis.

framework is used to combine process-based model predictions and medium-resolution satellite images. Some previous studies have applied similar methods using empirical forest simulation models based on predictions of the rate of change of selected forest variables (Nyström et al. 2015; Lindgren et al. 2017; Lindgren et al. 2022a & 2022b), whereas other studies utilising DA with forest data have applied static models for estimating the current state of forest variables from EO data (Hou et al., 2019; McRoberts et al., 2022). While DA with static models is suitable for improving the estimation and monitoring of forest variables, for the purposes of forest inventory, an additional goal of DA with dynamic simulation models is to improve future projections of forest growth. The DA can provide both continuous updates of the input data on forest variables, and continuous calibration of model parameters (Mäkelä et al. 2020, Junttila et al., 2023). Using process-based instead of empirical simulation models allows us to take into account changing climate inputs as well as to integrate information about the physiological status of the forests, such as drought stress or pest disturbances (Bastos et al., 2020). Combining satellite-based predictions and model predictions will allow identification and better monitoring of areas where a disturbance occurred.

By means of PREBAS emulators, we could overcome the computational challenges (Dietze et al., 2013; Fer et al., 2018) of DA and we assimilated data over large areas. Without the use of emulators, the computational load of DA can be prohibitive, especially for complex process-based models. For simple process-based models, like PREBAS, DA could still be performed without the use of emulators, however we opted for the most efficient solution. The reliability of emulators in mimicking PREBAS outputs is conditional on the time step of DA and the ecosystem considered. For boreal forests, a DA time step of 3–5 years is suitable; in more productive and fast-growing ecosystems (such as tropical for<ests, where complex processes occur at higher temporal resolution), the emulator performances should be tested and, eventually, a shorter DA time step should be considered. With the increasing availability of free-of-charge medium-resolution (10–20 m) satellite datasets, annual or biannual monitoring frequency can be considered feasible even in areas with high cloud coverage.

Combining data assimilation with field measurements is always desirable as it would allow a continuous validation of the data-model integrated system and a better quantification of uncertainties. This applies to both the simulation model and the forest data estimation. PREBAS was previously calibrated and tested for Boreal forests using an extensive dataset (Minunno et al., 2019) and the uncertainty in his predictions has been studied (Mäkelä et al., 2020; Junttila et al., 2023). In addition, combined use of field measurements and remotely sensed datasets allow spatially explicit analysis of the results distribution. Integrating the framework implemented here in national forest inventory campaigns would improve forest monitoring of carbon balance and growth at country scale.

4.1. *Forest structural variables prediction and validation*

Forest state dynamically changes over time. Therefore, model

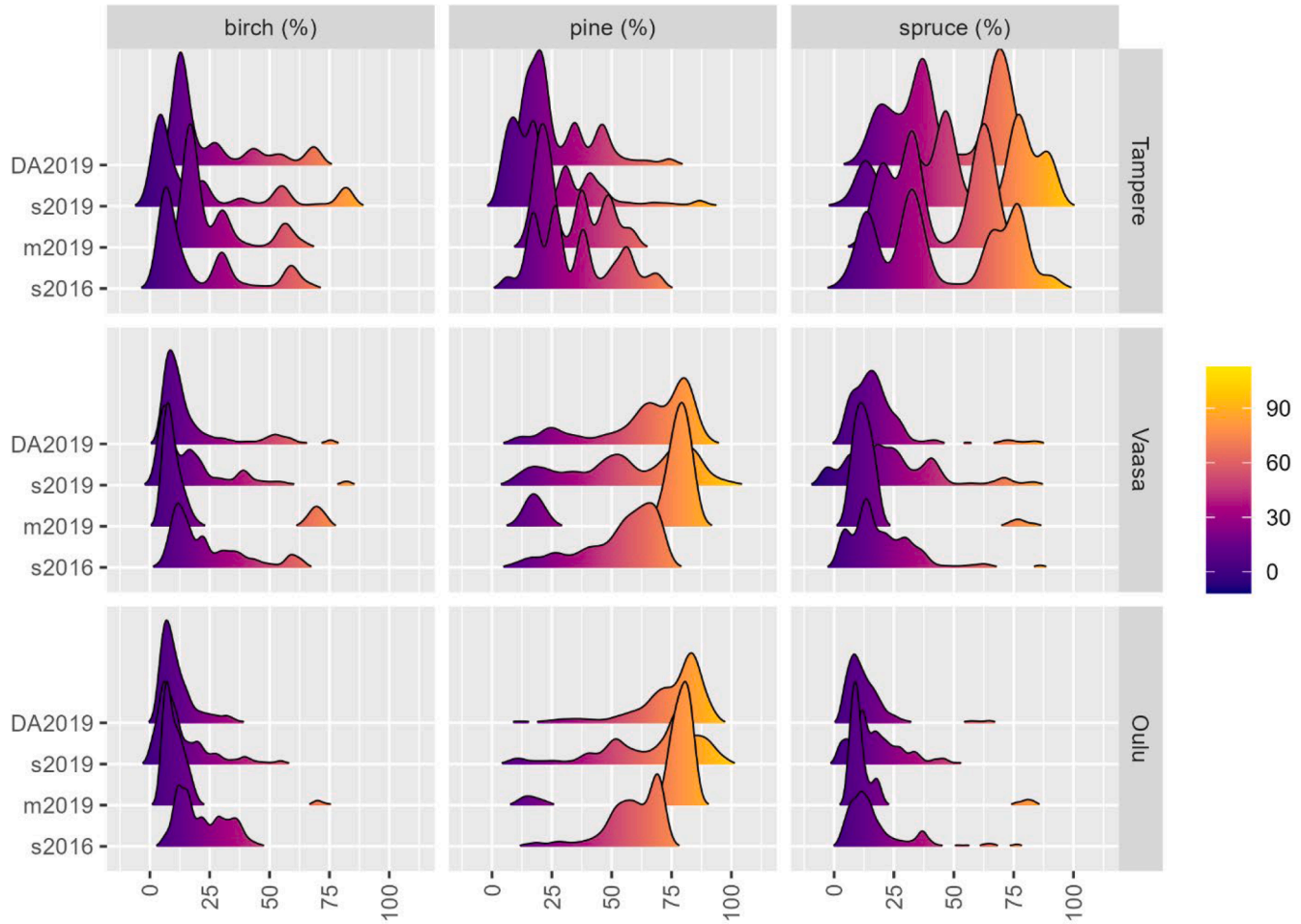

Fig. 6b. Distribution of deciduous species, pine, and spruce percentage cover over the three tiles using the highest probability predictions for each ground resolution element. The distributions were drawn from satellite-based predictions (s2016, s2019), model-based predictions (m2019), and data assimilation (DA2019). The color scale corresponds to the value of the x-axis.

predictions should integrate repeated measurements of forest status. Fusing information from both 2016 and 2019, using an ensemble Kalman filter, made our estimates more consistent and dependable. Satellite measurements and model predictions proved to be consistent (Fig. 10). Having satellite measurements that cover a longer time series could better inform the reliability of both model predictions and satellite-based predictions. This would allow identification of errors in the Earth observations or deficiencies in model structure. DA has the advantage of helping reduce and identify bias errors that could characterize both the initialization data and model predictions (Fox et al., 2018; Raczka et al., 2021). Potential biases in the initialization propagate through model forecasts. However, by means of data assimilation, the biases in the data can be easily identified and their impact becomes marginal once the DA process covers multiple data acquisitions. Our results show how data assimilation can increase the accuracy of forest monitoring. In fact, the impact of biased estimates of the last data acquisition (s2019) for D and H of the Oulu tile was limited in the data assimilation framework, because the weight of more accurate data (m2019) prevailed.

In comparison with satellite-based predictions in 2019, data assimilation results showed clearly lower predictive uncertainty, as the probability density distribution was shifting to a high kurtosis. The uncertainty was reduced because the product of two multivariate normal PDFs is proportional to the PDF of another multivariate distribution of smaller variance. In our analysis, we considered only the uncertainty in the initial state, as this is a major source of uncertainty (Makela et al., 2020; Kalliokoski et al. 2018). Although other sources of uncertainty, such as model parametric uncertainty, weather input uncertainty, and emulator uncertainty could be integrated in the data assimilation frameworks, we expect them to play a minor role considering the time interval of the consecutive measurements (3 years).

The uncertainty of the first measurements (s2016) was propagated to 2019 model forecasts (m2019). Some of the structural variables, namely D and H, showed a clear reduction of uncertainty for m2019. Possible reasons for this behaviour are that we considered forests where any management intervention was applied and H and D tend to reach a plateau across the rotation. In contrast, basal area uncertainty in m2019 predictions increased for the Tampere and Vaasa tiles and remained almost unchanged for Oulu, the northernmost tile, where the growth rates are lower. Basal area development depends on more complex processes, such as species interaction and natural mortality. These aspects would explain the increase in uncertainty of G in model predictions. Due to the integration in the modelling framework of the Sentinel-2 data of 2019, the uncertainty of basal area estimates was reduced.

The results of the validation show that the accuracy of the satellite-based estimates are consistent with previous studies (Häme et al. 2013; Sirro et al. 2018; Astola et al. 2019). Data assimilation and the most recent data acquisition performed better than PREBAS forecasts (m2019) for the southernmost tiles. The first data acquisition (s2016) was less accurate than the second (s2019), which is believed to be caused at least partially by the lower quality of the 2016 composite images, and the error was propagated through model predictions. The accuracy assessment of the Sentinel-2 based predictions was performed

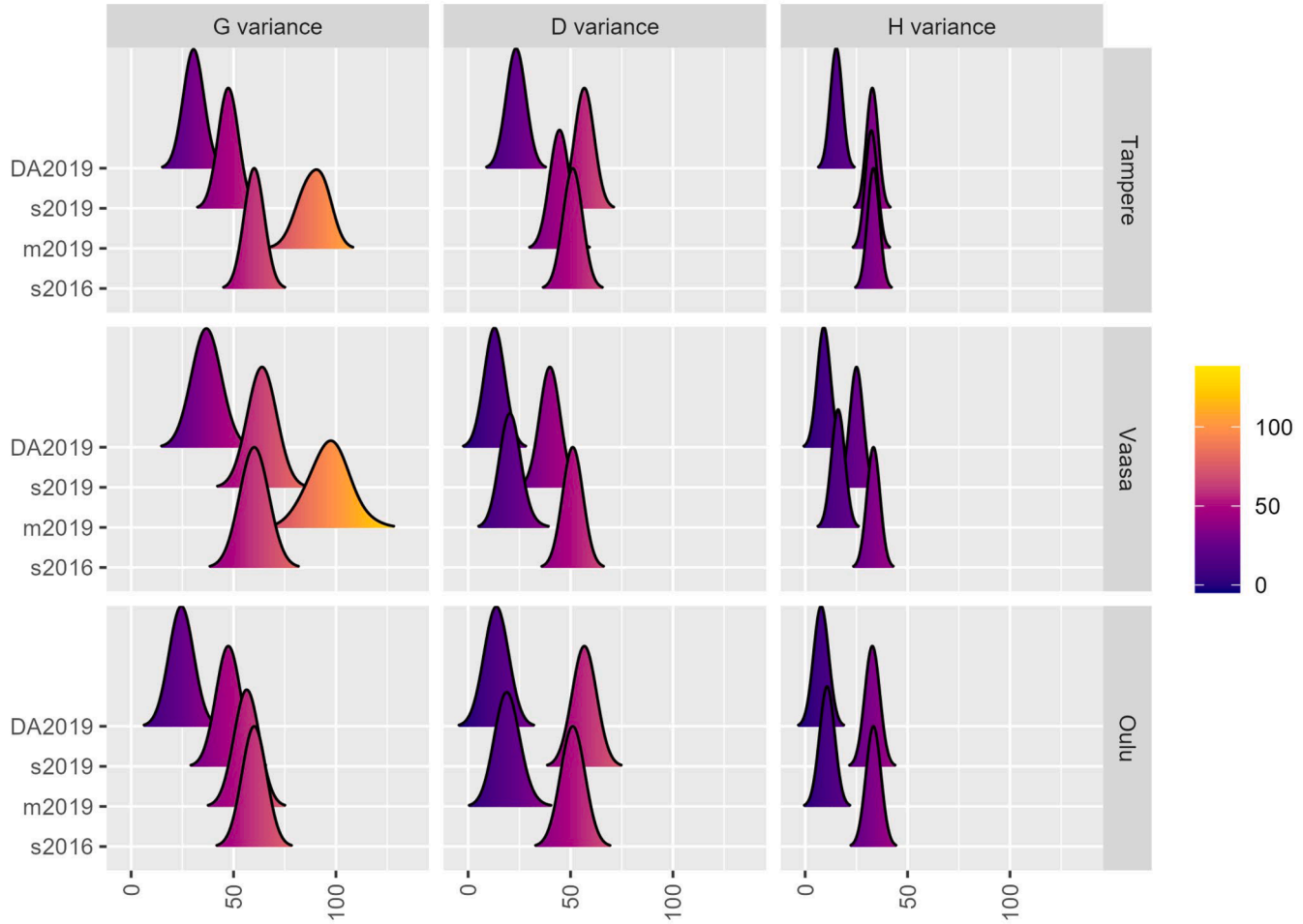

Fig. 7a. Variance distributions of basal area (*G*), average diameter at breast height (*D*), and average height (*H*) over the three tiles. For each spatial unit (10m x 10 m) we calculated the variance. The distributions were drawn from satellite-based predictions (s2016, s2019), model-based predictions (m2019), and data assimilation (DA2019) maps of variances calculated at spatial unit (10 × 10m). The color scale corresponds to the value of the x-axis.

using the testing plots [Table 1], see Miettinen et al. (2021) for details. Regarding the accuracy statistics, it must also be noted that the type of field plots used as reference data in this study may not be optimal for evaluating the accuracy of remote sensing based products. It is not expected to have affected the comparative analysis performed in this study, but the overall level of accuracy may be affected by the scale mismatch between pixel-level outputs and the field measurements. Larger plots (covering multiple pixels) or wall-to-wall reference data (derived e.g. from LiDAR scanning) could be more optimal for evaluation of the accuracy of Sentinel-2 based predictions.

Species proportions were the variables with higher error, but the impact of this error on forest growth is marginal since we modelled only 3 years. A more extensive test of the framework would be desirable especially for a longer period. Additional years should be included in the analyses, indeed, 3 years is rather short considering that the rotation length in the Boreal region is typically 80–100 years. In this study, the analyses were performed at 10 m x 10 m resolution. Future research should investigate at which level data assimilation should be implemented. Working at stand level and identifying homogeneous forested areas in terms of structure and management (Haakana et al. 2022) should be considered.

One important issue that needs further investigation for large area monitoring is the averaging tendency of EO based forest variable prediction. It is well known that empirical EO based prediction methods tend to gravitate towards the average, providing nearly unbiased results with representative reference data for large areas, but generally overestimating structural variables in regeneration areas and underestimating in voluminous forests (Lindgren et al. 2022a). Although recent investigation with UNet deep learning models show promising results on reducing the underestimation in high volume forests (Ge et al. 2022), the issue remains a problem for most applications. For this reason, the resulting map may have unrealistic size distribution of forests, overestimating the proportion of mid-size forests. This may have a significant effect on large area estimates if the maps are used as input in dynamic simulation models, as the model will propagate the initial errors over the time interval. If the subsequent EO estimates manifest the same error structure, this will also be transferred to the model, and the problem cannot be remedied with assimilating the erroneous data with the model using the same data.

Lindgren et al., 2022a, suggested to use classical calibration error to improve the DA process. Using this approach, it is possible to reduce systematic deviations between predictions based on remote sensing and the true values (Lindgren et al., 2022b). In appendix A3 we present DA results using the error calibration and further discuss the integration of this approach in DA process. We expect that the benefits of the error calibration to DA should increase with the number of data acquisitions (Lindgren et al. 2022a). Other recent studies showed the importance of accounting for forest variable correlations (Hou et al., 2019) and spatial autocorrelations and heteroscedasticity of the residuals (Xu et al., 2023) for improving DA accuracy and reducing the uncertainty of the predictions.

Furthermore, satellite-based predictions could be improved if

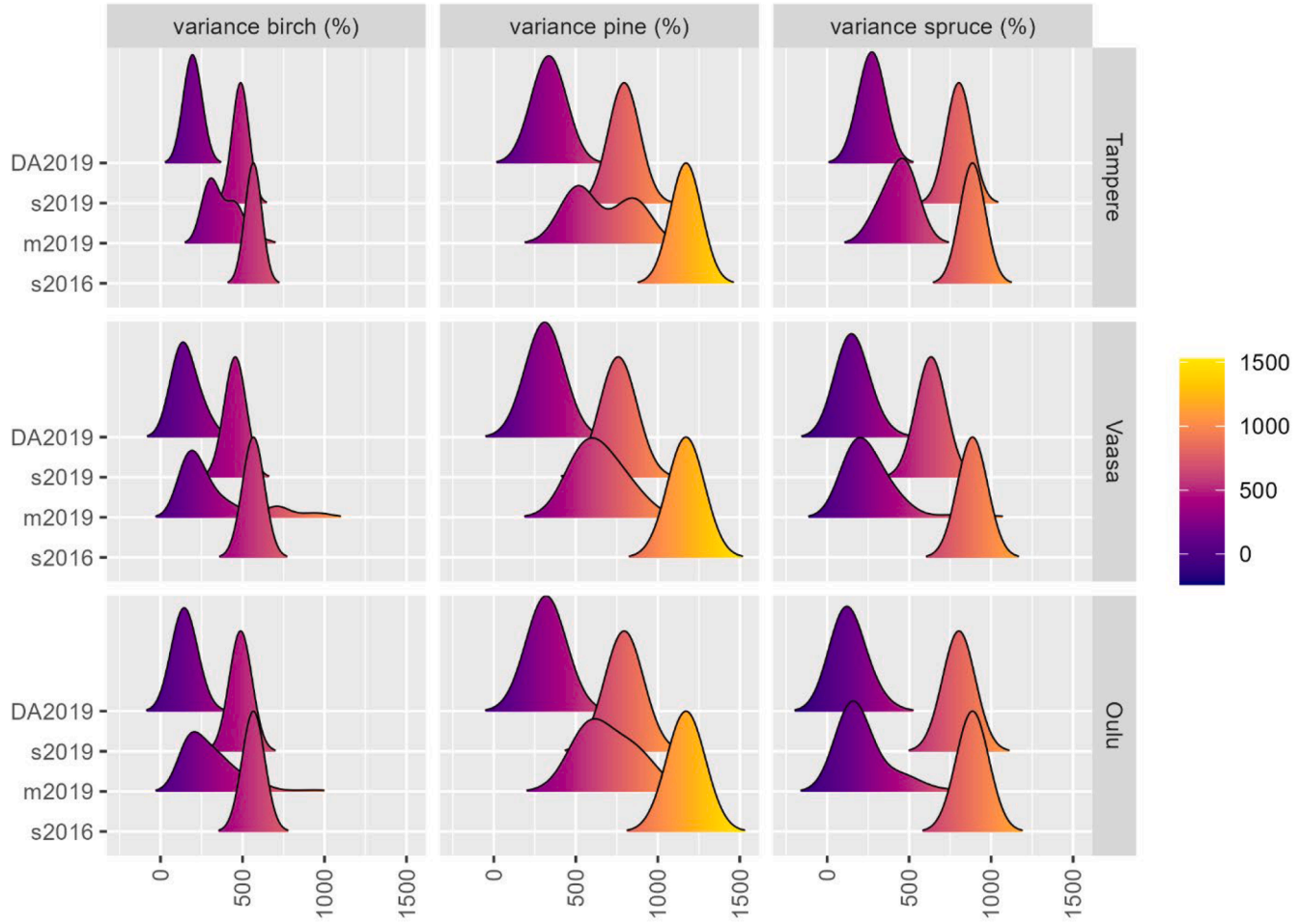

Fig. 7b. Variance distributions of species percentage cover over the three tiles. The distributions were drawn from satellite-based predictions (s2016, s2019), model-based predictions (m2019), and data assimilation (DA2019) maps of variances calculated at spatial unit (10 m x 10 m). The color scale corresponds to the value of the x-axis.

correlated errors between subsequent predictions based on EO data are taken into account (Ehlers et al., 2018). Taking into to account of error correlation seems to be particularly relevant for estimates based on optical satellite data (Reese et al., 2003; Tomppo et al., 2008). In this study, the field measurements were not collected at the same sites for this reason error correlation was not considered.

4.2. Site class data assimilation

Growth prediction in process-based models is based on climatic and edaphic factors, where the latter can be simplified to site fertility class (Mäkelä et al., 2023). While climate data and climate scenarios for future predictions are generally available globally (Carvalho et al. 2022), site fertility class manifests such small-scale variability that it is not available from, e.g., global or regional soil maps (Dai et al. 2019) but could be well covered by the 10–30 m resolution of the EO data of this study. Our idea in incorporating site fertility class in the DA process was to develop a method that would, in the long term, provide a means for estimating site fertility class from repeated EO predictions using our process-based model. Given the state of the stand and climate, the model prediction of future growth - at least in undisturbed stands - is largely determined by site fertility class. In the short term, and especially in the just 3-year time interval used in this study, uncertainties in the structural variables can be sufficiently large to mask any growth differences caused by site fertility class. In our results, therefore, the model simulation added little new insight into the analysis. However, we believe that the weight of model forecasts on data assimilation should increase when the analysis covers a longer period, in the order of decades for the Boreal region.

4.3. Future development

Data assimilation provides the opportunity to utilize the available information to update the state of forests. Data integration can be repeated systematically over time, providing a useful tool for forest monitoring and management planning (Saad et al., 2017). Future applications of DA based on dynamic forest simulation models also include improved forest growth and carbon balance projections, where process-based models can be used for predictions under climate change and exposure to multiple stressors. In this study, we used satellite-based predictions at medium resolution; in the framework implemented here, multiple data sources can be integrated at different spatial (from landscape to country scale) and temporal resolutions. For instance, national forest inventories, eddy-covariance fluxes, lidar, and unmanned aerial vehicle (UAV) data are some of the information sources that may also be included in the data assimilation process. Combining RS predictions from different sensors (i.e., multispectral data, 3D airborne laser scanning data and interferometric radar data) would improve the accuracy of RS predictions and DA (Ehlers et al., 2018).

The strength of data assimilation can be fully exploited when data from different sources and of different accuracy are used. We live in an era where a large volume of data is available. DA is a tool that allows

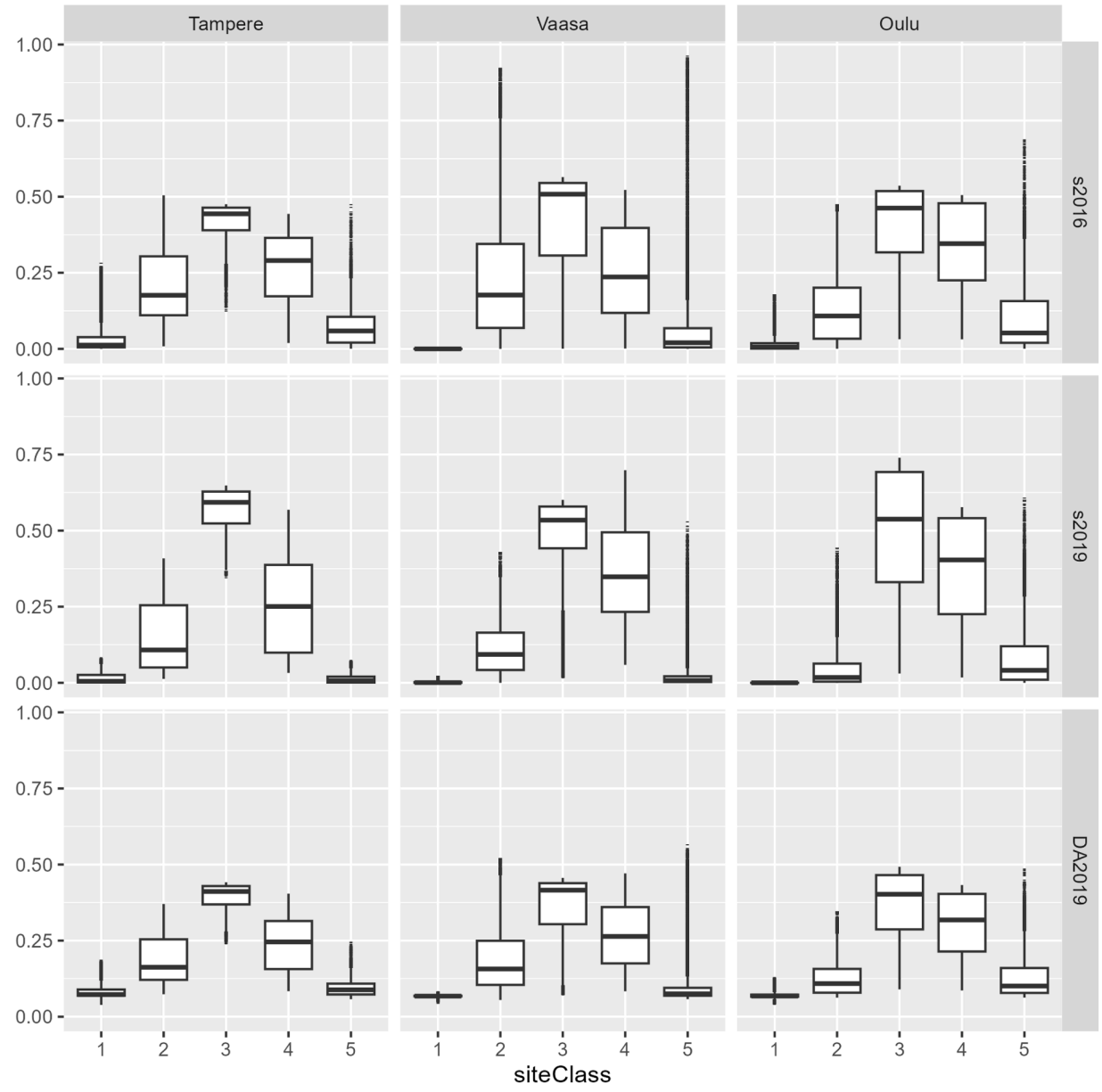

Fig. 8. Distribution of site fertility class for the different tiles. Satellite-based predictions for 2016 and 2019 (s2016 and s2019), and data assimilation results (DA2019) are reported. For each spatial unit, we calculated the probability of each fertility class of being the correct one based on the different sources of information (s2016, s2019 and DA2019). The boxplots represent the distribution of the site fertility class across the tiles.

Table 1
Characteristics of field data used for training and testing. Mean and standard deviation (sd) are reported for each variable and each year.

Year	Purpose	Plots (N)	Statistics	G (m^2/ha)	D (cm)	H (m)	V (m^3)	R_P (%)	R_S (%)	R_B (%)
2016	Training	1672	mean	18.4	16.5	14.0	148.9	49.6	28.0	20.3
			sd	10.4	8.0	6.5	117.0	41.7	35.2	30.2
	Testing	836	mean	17.8	16.4	13.9	143.3	50.1	28.5	19.5
			sd	10.0	8.1	6.6	114.6	41.8	35.3	29.2
2019	Training	1697	mean	18.5	16.4	14.3	152.6	44.4	30.4	23.4
			sd	10.5	8.5	6.9	124.8	41.3	35.6	32.0
	Testing	849	mean	18.6	16.5	14.3	153.9	44.2	30.4	23.1
			sd	10.7	8.6	6.8	125.2	41.9	36.2	32.2

combining models with field measurements, such as forest field measurements, remotely sensed data from optical and radar sensors, and any other source of data. The frameworks presented here can be applied with any kind of model and data and have great potential for future applications.

5. Conclusions

We implemented two DA frameworks for site fertility and forest structural variable predictions based on 10 m resolution EO data and a process-based growth model. The emulation of the forest growth model

Table 2
Finnish site fertility classes used in the study to describe fertility level.

Site type code	Finnish name	English translation
Site-1	Lehto	Herb-rich forest
Site-2	Lehtomainen kangas	Herb-rich heath forest
Site-3	Tuore kangas	Mesic heath forest
Site-4	Kuivahko kangas	Sub-xeric heath forest
Site-5	Kuiva kangas	Xeric heath forest

was required to reduce the computational load, even if the process-based model used here is relatively simple.

DA of forest structural variables reduced the uncertainty of the predictions, improved the accuracy of the forest structural variables and reduced the impact of biased data. However, for future applications, it will be important to increase the accuracy of satellite based predictions, reducing the systematic deviations from true values.

The frameworks developed here can be applied to any kind of model and data. A more extensive application of the framework using data of different uncertainties and longer period simulations is desirable to explore the full potential of the method.

CRediT authorship contribution statement

Francesco Minunno: Writing – review & editing, Writing – original

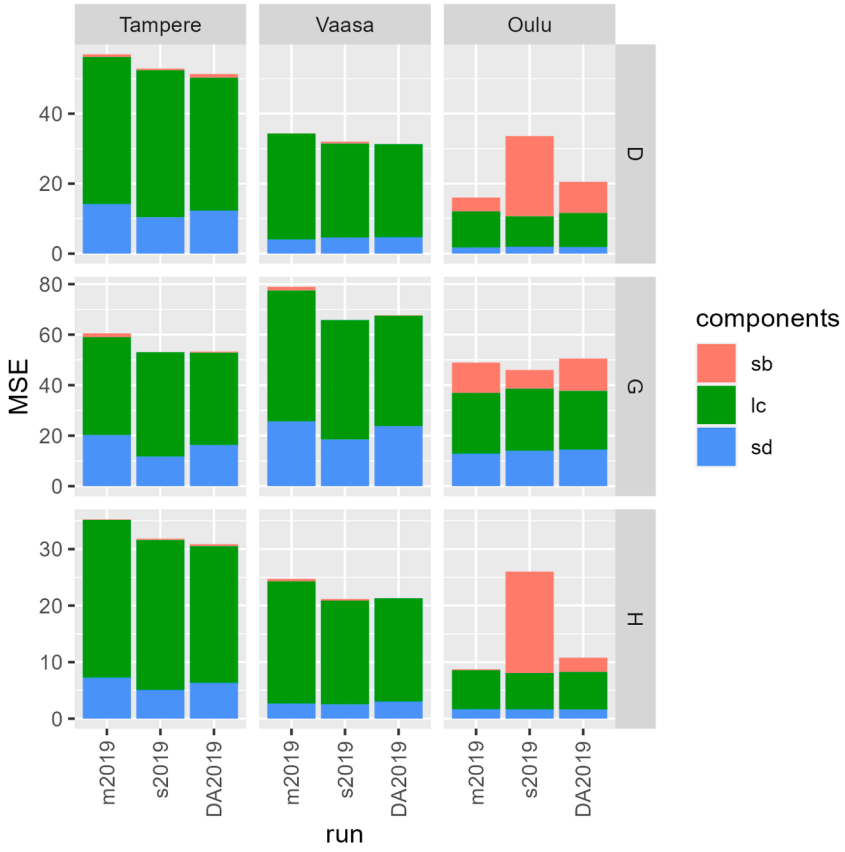

Fig. 9. Mean squared errors (MSE) for the forest structural variable estimates based on model forecasts (m2019), Sentinel-2 data of 2019 (s2019), and data assimilation of m2019 and s2019 (DA2019). Mean squared error was decomposed in three components: bias (s_b), data variability (s_d), and lack of correlation (l_c).

Table 3a
Root mean square error vs field-derived estimates for G, H and D based on DA2019, s2019, and m2019 predictions, see notation in Fig. 9.

RMSE	*G* (m^2 ha^{-1})			*H* (m)			*D* (cm)		
	m2019	s2019	DA2019	m2019	s2019	DA2019	m2019	s2019	DA2019
Tampere	7.8	7.3	7.3	5.9	5.6	5.6	7.5	7.3	7.2
Vaasa	8.9	8.1	8.2	5.0	4.6	4.6	5.9	5.7	5.6
Oulu	7.0	6.8	7.1	3.0	5.1	3.3	4.0	5.8	4.5

Table 3b
Percentage bias for G, H and D based on DA2019, s2019, and m2019 predictions, see notation in Fig. 9.

Bias	G (%)			H (%)			D (%)		
	m2019	s2019	DA2019	m2019	s2019	DA2019	m2019	s2019	DA2019
Tampere	−1.2	−0.1	−0.7	−0.3	−0.5	−0.6	−0.9	−0.7	−1.0
Vaasa	−1.2	0.0	−0.4	0.6	−0.5	0.2	0.2	−0.7	−0.2
Oulu	3.5	2.7	3.6	−0.4	−4.2	−1.6	−2.0	−4.8	−3.0

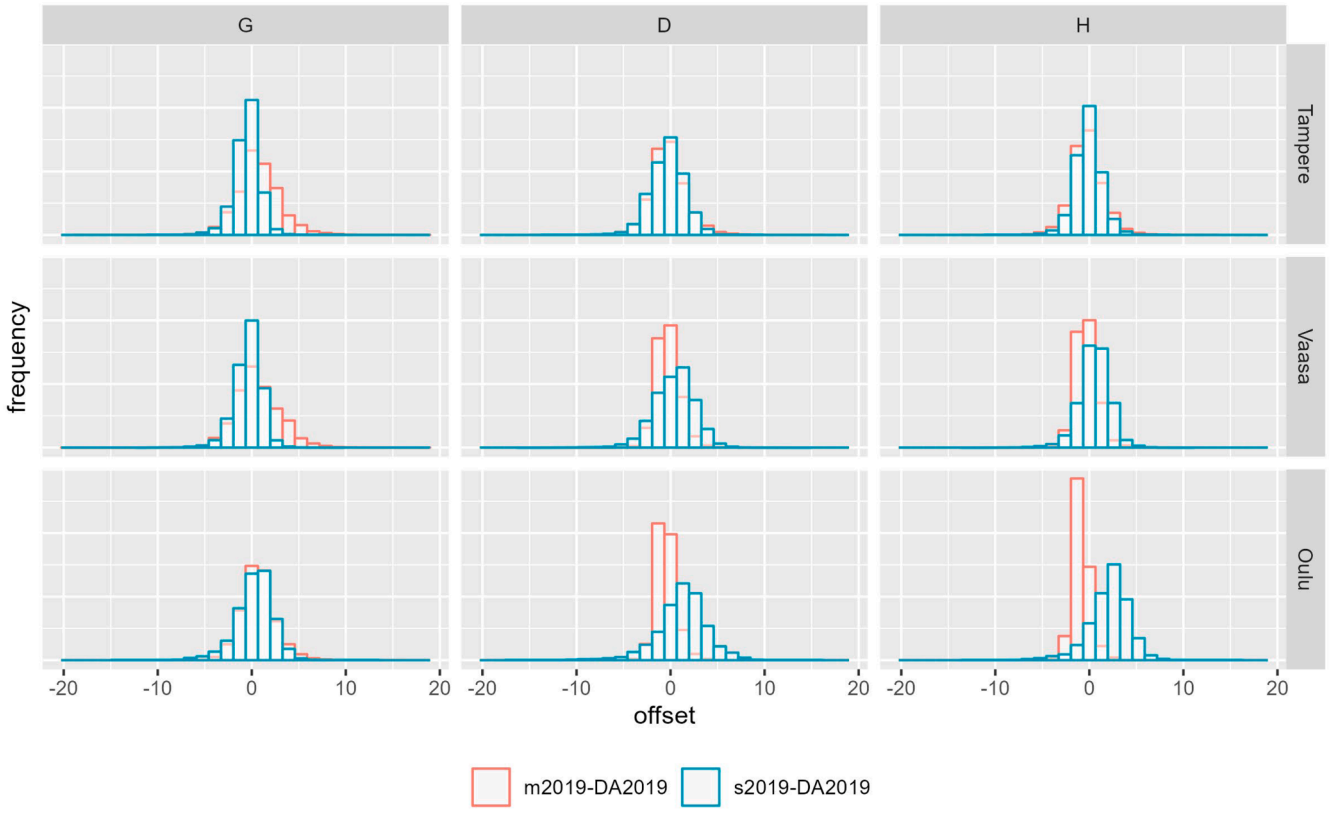

Fig. 10. Forest structural variables drawn using the *maximum a posteriori probability*. The distributions report the deviation between m2019 (red) and s2019 (blue) from DA2019 estimates at 10 meter resolution.

Table 4a
Root mean square error vs field-derived estimates for species proportion (R_p, R_s, R_b) based on DA2019, s2019, and m2019 predictions, see notation in Fig. 9.

RMSE	R_p (%)			R_s (%)			R_b (%)		
	m2019	s2019	DA2019	m2019	s2019	DA2019	m2019	s2019	DA2019
Tampere	37.4	28.0	31.0	34.0	28.9	30.8	27.4	23.1	23.7
Vaasa	37.8	28.2	30.6	29.8	25.3	26.6	26.2	21.7	22.1
Oulu	32.2	25.1	24.1	24.1	25.7	22.2	26.8	19.6	21.5

Table 4b
Percentage bias for species proportion (R_p, R_s, R_b) based on DA2019, s2019, and m2019 predictions, see notation in Fig. 9.

Bias	R_p (%)			R_s (%)			Rb (%)		
	m2019	s2019	DA2019	m2019	s2019	DA2019	m2019	s2019	DA2019
Tampere	−8.2	0.6	−4.0	8.4	−1.0	5.1	−1.4	−0.2	−2.3
Vaasa	−4.7	0.2	−3.0	1.4	−1.0	0.3	2.9	1.3	2.2
Oulu	−16.0	11.9	−3.8	2.2	−16.3	−4.5	13.8	5.0	8.3

Table 5
Counts of corrected predictions of site fertility classes.

Site Fertility Class	S2–2016 predictions	S2–2019 predictions	DA predictions
1	0 (0 %)	0 (0 %)	0 (0 %)
2	13 (12 %)	39 (36 %)	16 (15 %)
3	203 (90 %)	149 (66 %)	145 (64 %)
4	26 (17 %)	89 (58 %)	90 (59 %)
5	0 (0 %)	0 (0 %)	1 (5 %)
Tot	242 (55 %)	276 (63 %)	252 (57 %)

draft, Methodology, Formal analysis, Data curation, Conceptualization. **Jukka Miettinen:** Writing – review & editing, Writing – original draft, Funding acquisition, Formal analysis, Data curation, Conceptualization. **Xianglin Tian:** Writing – original draft, Data curation, Conceptualization. **Tuomas Häme:** Funding acquisition, Conceptualization. **Jonathan Holder:** Writing – original draft, Data curation. **Kristiina Koivu:** Data curation. **Annikki Mäkelä:** Writing – review & editing, Funding acquisition.

Declaration of competing interest

The authors declare that they have no known competing financial interests or personal relationships that could have appeared to influence the work reported in this paper

Acknowledgements

The authors would like to thank the European Space Agency (Assesscarbon project, Contract # 4000129960/20/I-DT; Forest Carbon Monitoring, Contract # 4000135015/21/I-NB), the European Union (H2020 ForestFlux project, Grant # 821860), and the Strategic Council of the Academy of Finland (Grant #335958) for funding that made this study possible.

Supplementary materials

Supplementary material associated with this article can be found, in the online version, at doi:10.1016/j.agrformet.2025.110436.

Data availability

I have shared the link with (part of the) data and codes.

References

Ahmadi, K., Kalantar, B., Saeidi, V., Harandi, E.K.G., Janizadeh, S., Ueda, N., 2021. Comparison of machine learning methods for mapping the stand characteristics of temperate forests using multi-spectral sentinel-2 data. Remote Sens. (Basel) 12, 3019. https://doi.org/10.3390/rs12183019.

Antropov, O., Rauste, Y., Häme, T., Praks, J., 2017. Polarimetric ALOS PALSAR time series in mapping biomass of boreal forests. Remote Sens. (Basel) 9, 999. https://doi.org/10.3390/rs9100999.

Astola, H., Häme, T., Sirro, L., Molinier, M., Kilpi, J., 2019. Comparison of Sentinel-2 and Landsat 8 imagery for forest variable prediction in boreal region. Remote Sens. Environ. 223, 257–273. https://doi.org/10.1016/J.RSE.2019.01.019.

Bastos, A., et al., 2020. Direct and seasonal legacy effects of the 2018 heat wave and drought on European ecosystem productivity. Sci. Adv. 6, eaba2724. https://doi.org/10.1126/sciadv.aba2724.

Breidenbach, J., Granhus, A., Hylen, G., et al., 2020. A century of national forest inventory in Norway – informing past, present, and future decisions. For. Ecosyst. 7, 46. https://doi.org/10.1186/s40663-020-00261-0.

Cajander, A.K., 1949. Finnish forest types and their significance. Acta For. Fenn. 56 (5), 1–71.

Calvet, J.C., de Rosnay, P., Penny, S.G., 2019. Editorial for the special issue "assimilation of remote sensing data into Earth system models. Remote Sens. 11, 2177. https://doi.org/10.3390/rs11182177, 2019.

Carvalho, D., Rafael, S., Monteiro, A., Rodrigues, V., Lopes, M., Rocha, A., 2022. How well have CMIP3, CMIP5 and CMIP6 future climate projections portrayed the recently observed warming. Sci. Rep. 12, 11983. https://doi.org/10.1038/s41598-022-16264-6.

Dai, Y., Shangguan, W., Wei, N., Xin, Q., Yuan, H., Zhang, S., Liu, S., Lu, X., Wang, D., Yan, F., 2019. A review of the global soil property maps for Earth system models. Soil. 5, 137–158. https://doi.org/10.5194/soil-5-137-2019.

Dietze, M.C., Lebauer, D.S., Kooper, R., 2013. On improving the communication between models and data. Plant Cell Environ. 36 (9), 1575–1585. https://doi.org/10.1111/pce.12043.

Ehlers, S., Saarela, S., Lindgren, N., Lindberg, E., Nyström, M., Persson, H.J., Olsson, H., Ståhl, G., 2018. Assessing error correlations in remote sensing-based estimates of forest attributes for improved composite estimation. Remote Sens. 10, 667. https://doi.org/10.3390/rs10050667.

Eriksson, L.O., Bergh, J.A., 2022. Tool for long-term forest stand projections of Swedish forests. Forests 13, 816. https://doi.org/10.3390/f13060816.

European Commission, 2019. The European green deal. communication from the European commission. COM 640, 2019.

Fer, I., Kelly, R., Moorcroft, P.R., Richardson, A.D., Cowdery, E.M., Dietze, M.C., 2018. Linking big models to big data: efficient ecosystem model calibration through bayesian model emulation. Biogeosciences 15 (19), 5801–5830. https://doi.org/10.5194/BG-15-5801-2.

Fontes, L., Bontemps, J.D., Bugmann, H., Van Oijen, M., Gracia, C., Kramer, K., Lindner, M., Roetzer, T., Skovsgaard, J.P., 2010. Models for supporting forest management in a changing environment. For. Syst. 19, 8–29.

Fox, A.M., Hoar, T.J., Anderson, J.L., Arellano, A.F., Smith, W.K., Litvak, M.E., et al., 2018. Evaluation of a data assimilation system for land surface models using CLM4.5. J. Adv. Model Earth Syst. 10, 2471–2494. https://doi.org/10.1002/2018MS001362.

Ge, S., Gu, H., Su, W., Praks, J., Antropov, O., 2022. Improved semisupervised UNet deep learning model for forest height mapping with satellite SAR and optical data. IEEE J. Selecte Topic. Appl. Earth Observ. Remote Sens. 15, 5776–5787. https://doi.org/10.1109/JSTARS.2022.3188201.

Haakana, M., Tuominen, S., Heikkinen, J., Peltoniemi, M., Lehtonen, A., 2022. Spatial patterns of biomass change across Finland in 2009–2015. https://doi.org/10.1101/2022.02.15.480479 bioRxiv preprint.

Häme, T., 1984. Landsat-aided forest site type mapping. Photogr. Eng. Rem. Sens. 1175–1183, 1984.

Häme, T., Astola, H., Kilpi, J., Rauste, Y., Sirro, L., Mutanen, T., Parmes, E., Rasinmäki, J., Imangholiloo, M., 2023. Forest area and structural variable estimation in Boreal Forest using Suomi NPP VIIRS data and a sample from VHR Imagery. Remote Sens. (Basel) 15 (12), 3029. https://doi.org/10.3390/RS15123029, 2023Page153029.

Häme, T., Stenberg, P., Andersson, K., Rauste, Y., Kennedy, P., Folving, S., Sarkeala, J., 2001. AVHRR-based forest proportion map of the Pan-European area. Remote Sens. Environ. 77 (1), 76–91.

Häme, T., Kilpi, J., Ahola, H., Rauste, Y., Antropov, O., Rautiainen, M., Sirro, L., Bounepone, S., 2013. Improved mapping of tropical forests with optical and SAR imagery, part I: forest cover and accuracy assessment using multi-resolution data. IEEE J. Select. Topic. Appl. Earth Obs. Remote Sens. 6, 74–91.

Hou, Z., Mehtätalo, L., McRoberts, R.E., Ståhl, G., Tokola, T., Rana, P., Siipilehto, J., Xu, Q., 2019. Remote sensing-assisted data assimilation and simultaneous inference for forest inventory. Remote Sens. Environ. 234, 111431. https://doi.org/10.1016/j.rse.2019.111431. VolumeISSN 0034-4257.

Hynynen, J., Ojansuu, R., Hökkä, H., Siipilehto, J., Salminen, H., Haapala, P., 2002. Models for predicting stand development in MELA system. Finnish For. Res. Institute Res. Papers 835, 116. http://urn.fi/URN:ISBN:951-40-1815-X.

Junttila, V., Maltamo, M., Kauranne, T., 2008. Sparse bayesian estimation of forest stand characteristics from airborne laser scanning. For. Sci. 54, 543–552. https://doi.org/10.1093/forestscience/54.5.543.

Junttila, V., Minunno, F., Peltoniemi, M., et al., 2023. Correction to: quantification of forest carbon flux and stock uncertainties under climate change and their use in regionally explicit decision making: case study in Finland. Ambio 52, 1734–1736. https://doi.org/10.1007/s13280-023-01919-z.

Kallio, A.M.I., Salminen, O., Sievänen, R., 2016. Forests in the Finnish low carbon scenarios. J. For. Econ. 23, 45–62. https://doi.org/10.1016/j.jfe.2015.12.001.

Kalliokoski, T., Mäkelä, A., Fronzek, T., Minunno, F., Peltoniemi, M., 2018. Decomposing sources of uncertainty in climate change projections of boreal forest primary production. Agric. For. Meteorol. 262, 192–205.

Kangas, A., Astrup, R., Breidenbach, J., Fridman, J., Gobakken, T., Korhonen, K.T., Maltamo, M., Nilsson, M., Nord-Larsen, T., Næsset, E., Olsson, H., 2018. Remote sensing and forest inventories in Nordic countries – roadmap for the future. Scand. J. For. Res. 33, 397–412. https://doi.org/10.1080/02827581.2017.1416666.

Khaki, M., Hendricks Franssen, H.-J., Han, S.C., 2020. Multimission satellite remote sensing data for improving land hydrological models via data assimilation. Sci. Rep. 10, 18791. https://doi.org/10.1038/s41598-020-75710-5. |.

Knyazikhin, Y., Schull, M.A., Stenberg, P., Möttus, M., Rautiainen, M., Yang, Y., Marshak, A., Latorre Carmona, P., Kaufmann, R.K., Lewis, P., Disney, M.I., Vanderbilt, V., Davis, A.B., Baret, F., Jackuemoud, S., Lyapustin, A., Myneni, R.B., 2013. Hyperspectral remote sensing of foliar nitrogen content. Proc. Natl Acad. Sci. 110, E185–E192.

Kobayashi, K., Salam, M.U., 2000. Comparing simulated and measured values using mean squared deviation and its components. Agron. J. 92, 345–352. https://doi.org/10.2134/agronj2000.922345x.

Korhonen, K.T., Ihalainen, A., Ahola, A., Heikkinen, J., Henttonen, H.M., Hotanen, J.-P., Nevalainen, S., Pitkänen, J., Strandström, M., Viiri, H. 2017. Suomen metsät 2009–2013 ja niiden kehitys 1921–2013 (Finland's forests 2009-2013 and their development 1921-2013. In Finnish). Publ. Nat. Res. Inst. Finland 59/2917. 86 pp. http://urn.fi/URN:ISBN:978-952-326-467-0.

Lämås, T., Sängstuvall, L., Öhman, K., Lundström, J., Årevall, J., Holmström, H., Nilsson, L., Nordström, E.-M., Wikberg, P.-E., Wikström, P., Eggers, J., 2023. Themulti-faceted Swedish Heureka forestdecision support system: context, functionality, design, and 10 years experiencesof its use. Front. For. Glob. 6, 1163105. https://doi.org/10.3389/ffgc.2023.1163105. Change.

Leroux, D.J., Calvet, J.-C., Munier, S., Albergel, C., 2018. Using satellite-derived vegetation products to evaluate LDAS-Monde over the Euro-Mediterranean. Remote Sens. 10, 1199. https://doi.org/10.3390/rs10081199. **2018**.

Lindgren, N., Persson, H.J., Nyström, M., Nyström, K., Grafström, A., Muszta, A., Willén, E., Fransson, J.E.S., Ståhl, G., Olsson, H., 2017. Improved prediction of forest variables using data assimilation of interferometric synthetic aperture radar data. Can. J. Remote Sens. 43 (4), 374–383. https://doi.org/10.1080/07038992.2017.1356220.

Lindgren, N., Nyström, K., Saarela, S., Olsson, H., Ståhl, G., 2022a. Importance of calibration for improving the efficiency of data assimilation for predicting forest characteristics. Remote Sens. 14, 4627. https://doi.org/10.3390/rs14184627 a.

Lindgren, N., Olsson, H., Nyström, K., Nyström, M., Ståhl, G., 2022b. Data assimilation of growing stock volume using a sequence of remote sensing Data from different sensors. Can. J. Remote Sens. 48 (2), 127–143. https://doi.org/10.1080/07038992.2021.1988542.

Lucash, M.S., Scheller, R.M., Sturtevant, B.R., Gustafson, E.J., Kretchun, A.M., Foster, J. R., 2018. More than the sum of its parts: how disturbance interactions shape forest dynamics under climate change. Ecosphere 9 (6) e02293.10.1002/ecs2.2293.

Mäkelä, A., 1997. A carbon balance model of growth and self-pruning in trees based on structural relationships. For. Sci. 43 (1), 7–24.

Mäkelä, J., Minunno, F., Aalto, T., Mäkelä, A., Markkanen, T., Peltoniemi, M., 2020. Sensitivity of 21st century simulated ecosystem indicators to model parameters, prescribed climate drivers, RCP scenarios and forest management actions for two Finnish boreal forest sites. Biogeosciences 17, 2681–2700. https://doi.org/10.5194/bg-17-2681-2020.

Mäkelä, A., Minunno, F., Kujala, H., et al., 2023. Effect of forest management choices on carbon sequestration and biodiversity at national scale. Ambio 52, 1737–1756. https://doi.org/10.1007/s13280-023-01899-0.

Mäkelä, A., et al., 2007. Developing an empirical model of stand GPP with the LUE approach: analysis of eddy covariance data at five contrasting conifer sites in Europe.

Glob. Change Biol. 14, 92–108. https://doi.org/10.1111/j.1365-2486.2007.01463.x.
McRoberts, R.E., Næsset, E., Heikkinen, J., Chen, Q., Strimbu, V., Esteban, J., Hou, Z., Giannetti, F., Mohammadi, J., Chirici, G., 2022. On the model-assisted regression estimators using remotely sensed auxiliary data. Remote Sens. Environ. 281, 113168. https://doi.org/10.1016/j.rse.2022.113168.
McRoberts, R., Tomppo, E., Schadauer, K., Vidal, C., Ståhl, G., Chirici, G., Lanz, A., Cienciala, E., Winter, S., Smith, W.B., 2009. Harmonizing national forest inventories. J. For. 107, 179–187.
Minunno, F., van Oijen, M., Cameron, D.R., Cerasoli, S., Pereira, J.S., Tomé, M., 2013. Using a Bayesian framework and global sensitivity analysis to identify strengths and weaknesses of two process-based models differing in representation of autotrophic respiration. Environ. Modell. Softw. 42, 99–115. https://doi.org/10.1016/J.ENVSOFT.2012.12.010.
Minunno, F., Peltoniemi, M., Launiainen, S., Aurela, M., Mammarella, I., Lindroth, A., Lohela, A., Minkkinen, K., Mäkelä, A., 2016. Calibration and validation of a semi-empirical flux ecosystem model for coniferous forests in the Boreal region. Ecol. Modell. 341, 37–52.
Miettinen, J., Carlier, S., Häme, L., Mäkelä, A., Minunno, F., Penttilä, J., Pisl, J., Rasinmäki, J., Rauste, Y., Seitsonen, L., Tian, X., Häme, T., 2021. Demonstration of large area forest volume and primary production estimation approach based on Sentinel-2 imagery and process based ecosystem modelling. Int. J. Remote Sens. 42, 9492–9514. https://doi.org/10.1080/01431161.2021.1998715.
Minunno, F., Peltoniemi, M., Härkönen, S., Kalliokoski, T., Makinen, H., Mäkelä, A., 2019. Bayesian calibration of a carbon balance model PREBAS using data from permanent growth experiments and national forest inventory. For. Ecol. Manage. 440, 208–257.
Mohamedou, C., Kangas, A., Hamedianfar, A., Vauhkonen, J., 2022. Potential of Bayesian formalism for the fusion and assimilation of sequential forestry data in time and space. Can. J. For. Res. 52, 439–449. https://doi.org/10.1139/cjfr-2021-0145, 2022.
Montzka, C., Pauwels, V.R.N., Hendriks Franssen, H.-J., Han, X., Vereecken, H., 2012. Multivariate and multiscale data assimilation in terrestrial systems: a review. Sensors 12, 16291–16333. https://doi.org/10.3390/s121216291, 2012.
Moran, E.F., Brondizio, E.S., Tucker, J.M., Da Silva-Forsberg, M.C., McCracken, S., Falesi, I., 2000. Effects of soil fertility and land-use on forest succession in Amazônia. For. Ecol. Manage. 139 (1–3), 93–108. https://doi.org/10.1016/S0378-1127(99)00337-0.
Nabuurs, G.-J., Lindner, M., Verkerk, P.J., Gunia, K., Deda, P., Michalak, R., Grassi, G., 2013. First signs of carbon sink saturation in European forest biomass. Nat. Clim. Change 3, 792–796.
Nyström, M., Lindgren, N., Wallerman, J., Grafström, A., Muszta, A., Nyström, K., Bohlin, J., et al., 2015. Data assimilation in forest inventory: first empirical results. Forests 6 (12), 4540–4557. https://doi.org/10.3390/f6124384.
Peltoniemi, M., Pulkkinen, M., Aurela, M., Pumpanen, J., Kolari, P., Mäkelä, A., 2015. Boreal environment research : an international interdisciplinary journal. Retrieved from Boreal. Environ. Res. 20, 151–171.10138/228031.
Rabier, F., 2005. Overview of global data assimilation developments in numerical weather-prediction centres. Q. J. R. Meteorol. Soc. 131, 3215–3233.
Raczka, B., Hoar, T.J., Duarte, H.F., Fox, A.M., Anderson, J.L., Bowling, D.R., Lin, J.C., 2021. Improving CLM5.0 biomass and carbon exchange across the Western United States using a data assimilation system. J. Adv. Model. Earth Syst. 13. https://doi.org/10.1029/2020MS002421 e2020MS002421.
Rahimzadeh-Bajgiran, P., Hennigar, C., Weiskittel, A., Lamb, S., 2020. Forest potential productivity mapping by linking remote-sensing-derived metrics to site variables. Remote Sens. (Basel) 12 (12), 2056. https://doi.org/10.3390/RS12122056, 2020Page122056.
Reese, H., Nilsson, M., Pahén, T.G., Hagner, O., Joyce, S., Tingelöf, U., Egberth, M., Olsson, H., 2003. Countrywide estimates of forest variables using satellite data and field data from the National Forest Inventory. Ambio 32, 542–548. https://doi.org/10.1579/0044-7447-32.8.542. PMID:15049351.
Reyer, C.P.O., Bathgate, S., Blennow, K., Borges, J.G., Bugmann, H., Delzon, S., Faias, S. P., Garcia-Gonzalo, J., Gardiner, B., Gonzalez-Olabarria, J.R., Gracia, C., Hern_andez, J.G., Kellomäki, S., Kramer, K., Lexer, M.J., Lindner, M., van der Maaten, E., Maroschek, M., Muys, B., Nicoll, B., Palahi, M., Palma, J.H., Paulo, J.A., Peltola, H., Pukkala, T., Rammer, W., Ray, D., Sabat_e, S., Schelhaas, M.-J., Seidl, R., Temperli, C., Tom_e, M., Yousefpour, R., Zimmermann, N.E., Hanewinkel, M., 2017. Are forest disturbances amplifying or canceling out climate change-induced productivity changes in European forests? Environ. Res. Lett. 12, 34027. https://doi.org/10.1088/1748-9326/aa5ef1.
Saad, R., Eyvindson, K., Gong, P., Lämås, T., Ståhl, G., 2017. Potential of using data assimilation to support forest planning. Can. J. Forest Res. 47, 690–695. https://doi.org/10.1139/cjfr-2016-0439.
Sánchez-Ruiz, S., Moreno-Martínez, A., Izquierdo-Verdiguierd, E., Chiesi, M., Maselli, F., Gilabert, M.A., 2019. Growing stock volume from multi-temporal landsat imagery through google earth engine. Int. J. Appl. Earth Obs. Geoinf. 83, 101913. https://doi.org/10.1016/j.jag.2019.101913.
Santoro, M., Cartus, O., Fransson, J.E.S., Wegmüller, U., 2019b. Complementarity of X-, C-, and L-band SAR backscatter observations to retrieve forest stem volume in boreal forest. Remote Sens. (Basel) 11, 1563. https://doi.org/10.3390/rs11131563.
Sirro, L., Häme, T., Rauste, Y., Kilpi, J., Hämäläinen, J., Gunia, K., De Jong, B., Paz Pellat, F., 2018. Potential of different optical and SAR data in forest and land cover classification to support REDD+ MRV. Remote Sens. (Basel) 10, 942.
Skovsgaard, J.P., Vanclay, J.K., 2008. Forest site productivity: a review of the evolution of dendrometric concepts for even-aged stands. Forestry 81, 13–31.
Tomppo, E., 1992. Satellite image aided forest site fertility estimation for forest income taxation. Acta For. Fenn. (229). https://doi.org/10.14214/aff.7675 article id 7675.
Tomppo, E., Olsson, H., Ståhl, G., Nilsson, M., Hagner, O., Katila, M., 2008. Combining national forest inventory field plots and remote sensing data for forest databases. Remote Sens. Environ. 112, 1982–1999. https://doi.org/10.1016/j.rse.2007.03.032. ISSN 0034-4257.
Van Oijen, M., Reyer, C., Bohn, F.J., D.R:, Cameron, Deckmyn, G., Felchsig, M., Härkönen, S., Hartig, F., Huth, A., Kiviste, A., Lasch, P., Mäkelä, A., Mette, T., Minunno, F., Rammer, W, 2013. Bayesian calibration, comparison and averaging of six forest models, using data from Scots pine stands across Europe. For. Ecol. Manage. 289, 255–268.
Valentine, H.T., Mäkelä, A., 2005. Bridging process-based and empirical approaches to modeling tree growth. Tree Physiol. 25, 769–779.
Verkerk, P.J., Hassegawa, M., Van Brusselen, J., Cramm, M., Chen, X., Maximo, Y.I., Koç, M., Lovrić, M., Tegegne, Y.T., 2022. Forest Products in the Global Bioeconomy – *Enabling substitution By Wood-Based Products and Contributing to the Sustainable Development Goals*. FAO, Rome. https://doi.org/10.4060/cb7274en.
Vuokila, Y., Väliaho, H., 1980. Growth and Yield Models of Planted Conifer Forests (In Finnish). Publications of the Finnish Forest Research Institute, p. 271.
Waring, R., Landsberg, J., Linder, S., 2016. Tamm Review: insights gained from light use and leaf growth efficiency indices. For. Ecol. Manage. 379, 232–242.
Xu, Q., Li, B., McRoberts, R.E., Li, Z., Hou, Z., 2023. Harnessing data assimilation and spatial autocorrelation for forest inventory. Remote Sens. Environ. 288, 113488. https://doi.org/10.1016/j.rse.2023.113488. ISSN 0034-4257.